2001 CEDAR-SCOSTEP

Longmont, Colorado

June 17-22, 2001

Tutorial Lecture #3

by Joanna Haigh

Imperial College of Science,

Technology and Medicine, UK

Solar Influences on Global Climate Change and the IPCC Third Assessment Report

Overview:

- Greenhouse effect and radiative forcing
- Radiative forcing components in IPCC TAR
- Structure, remit and procedures of IPCC
- Solar signal in climate records
- Current uncertainties, theories, research

Radiation Balance

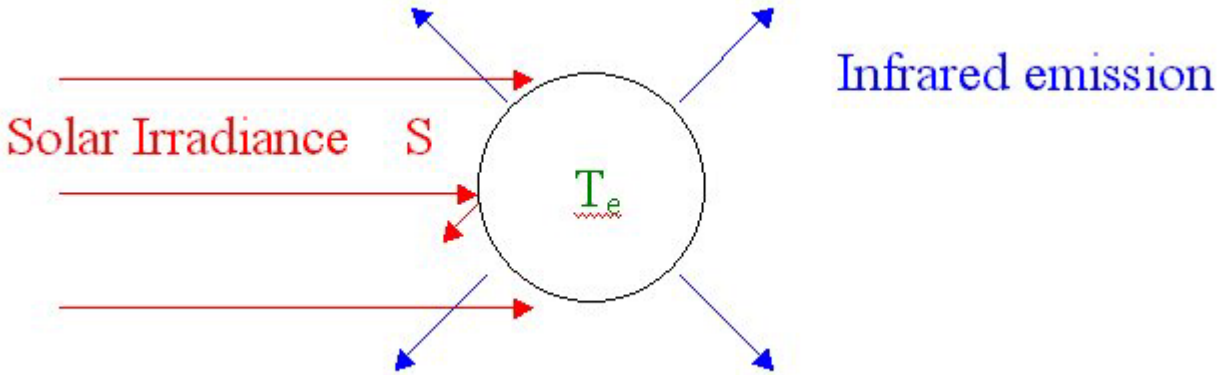

In equilibrium:

absorption solar radiation = emission infrared radiation:

$$\pi R^2 (1-\alpha) S = 4\pi R^2 \sigma T_e^{\,4}$$

$$\sigma T_e^{\,4} = (1-\alpha) S/4 = F_s$$

$$S = 1370 Wm^{-2} \quad F_s = 240 Wm^{-2} \quad T_e = 255K$$

Greenhouse Effect

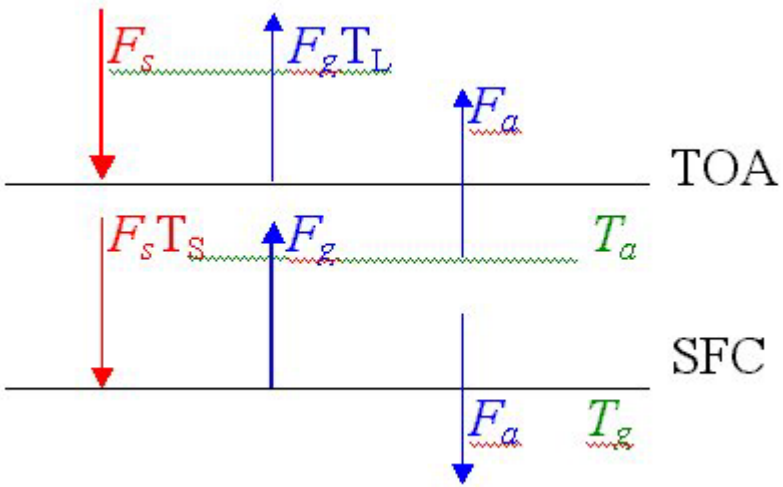

$$\text{TOA}: \quad F_S = \mathrm{T}_L F_g + F_a$$

$$\text{SFC}: \quad F_S \mathrm{T}_S = F_g - F_a$$

$$\therefore \quad F_g = \frac{(1+\mathrm{T}_S)}{(1+\mathrm{T}_L)} F_S$$

$$\text{i.e.} \quad T_g^{\,4} = \frac{(1+\mathrm{T}_S)}{(1+\mathrm{T}_L)} T_e^{\,4}$$

$$\therefore \quad \text{If} \quad \mathrm{T}_S > \mathrm{T}_L \quad \text{then} \quad T_g > T_e$$

Factors which affect equilibrium T_g:

T_e	S	Solar irradiance
T_e	α	Albedo: surface, cloud, aerosol, O_3
T_S		O_3, H_2O, NO_2, ……..
T_L		H_2O, CO_2, CH_4, N_2O, O_3, CFCs, ……(GHGs)

Radiative Forcing

Net downward flux at TOA is:

$$
\begin{aligned}
F_N^{\downarrow} &= F_S - \mathrm{T}_L F_g - F_a \\
&= \sigma T_e^{\,4} - \mathrm{T}_L \sigma T_g^{\,4} - (1 - \mathrm{T}_L)\sigma T_a^{\,4} \\
&= \sigma\left[T_e^{\,4} - \left(T_g^{\,4} - T_a^{\,4}\right)\mathrm{T}_L - T_a^{\,4}\right] \\
&= 0 \quad \text{in equilibrium}
\end{aligned}
$$

For given T_g, T_a

perturbations to T_e or $\mathrm{T}_L \rightarrow F_N^{\downarrow} \neq 0$

Define $\Delta \boldsymbol{F}_{\boldsymbol{N}}^{\downarrow} = \boldsymbol{RF}$ Radiative Forcing

Why is radiative forcing a useful concept?

Because GCMs, & limited observational studies, suggest that the perturbation in global average, equilibrium surface temperature:

$$\Delta T_g = \lambda \, RF$$

where λ, the climate sensitivity parameter, is independent of the nature of the forcing.

$$\lambda \sim 0.5 \text{ K W}^{-1} \text{ m}^2$$

Complications:

- Stratospheric adjustment:
  - $\Delta F_N^{\downarrow}$ at tropopause $\rightarrow$ less variation in λ
- Feedbacks:
  - H_2O, cloud, indirect aerosol, chemistry, ……
- Geographical and vertical distributions
- Equilibrium ΔT_g predicted

The Intergovernmental Panel on Climate Change (IPCC)

Established 1988 by:

World Meteorological Organization (WMO) & United Nations Environment Programme (UNEP)

Role:

To assess the scientific, technical and socio-economic information relevant for the understanding of the risk of human-induced climate change.

IPCC does not carry out new research nor does it monitor climate related data.

Assessments are based on published and peer reviewed scientific technical literature.

3 IPCC working groups:

- WG I assesses the scientific aspects of the climate system and climate change.
- WG II addresses the vulnerability of socio-economic and natural systems to climate change, negative and positive consequences of climate change, and options for adapting to it.
- WG III assesses options for limiting greenhouse gas emissions and otherwise mitigating climate change.

Membership of the Working Groups by invitation, nominations submitted by national governments. Membership changes between reports.

IPCC Reports:

First Assessment Report (FAR) 1990

Second Assessment Report (SAR) 1995

Third Assessment Report (TAR) 2001 (imminent)

plus several other special reports e.g.:

Radiative Forcing 1994

Aviation and the Global Atmosphere 1999

Emission Scenarios 2000

Third Assessment Report - Working Group I

~ 120 Lead Authors
~ 300 Contributing Authors
hundreds Reviewers

Timetable:

- Dec 1998 first meeting of WGs
- May 1999 0th draft complete
- Friendly review
- Jul 1999 1st drafting meting
- Sep 1999 1st draft complete
- Expert Review
- Feb 2000 2nd drafting meeting
- Mar 2000 2nd draft complete
- Expert & Government Reviews
- Aug 2000 3rd drafting meeting
- Oct 2000 Final draft complete
- Jan 2001 Accepted

Summaries and Synthesis Report written

Table of Contents

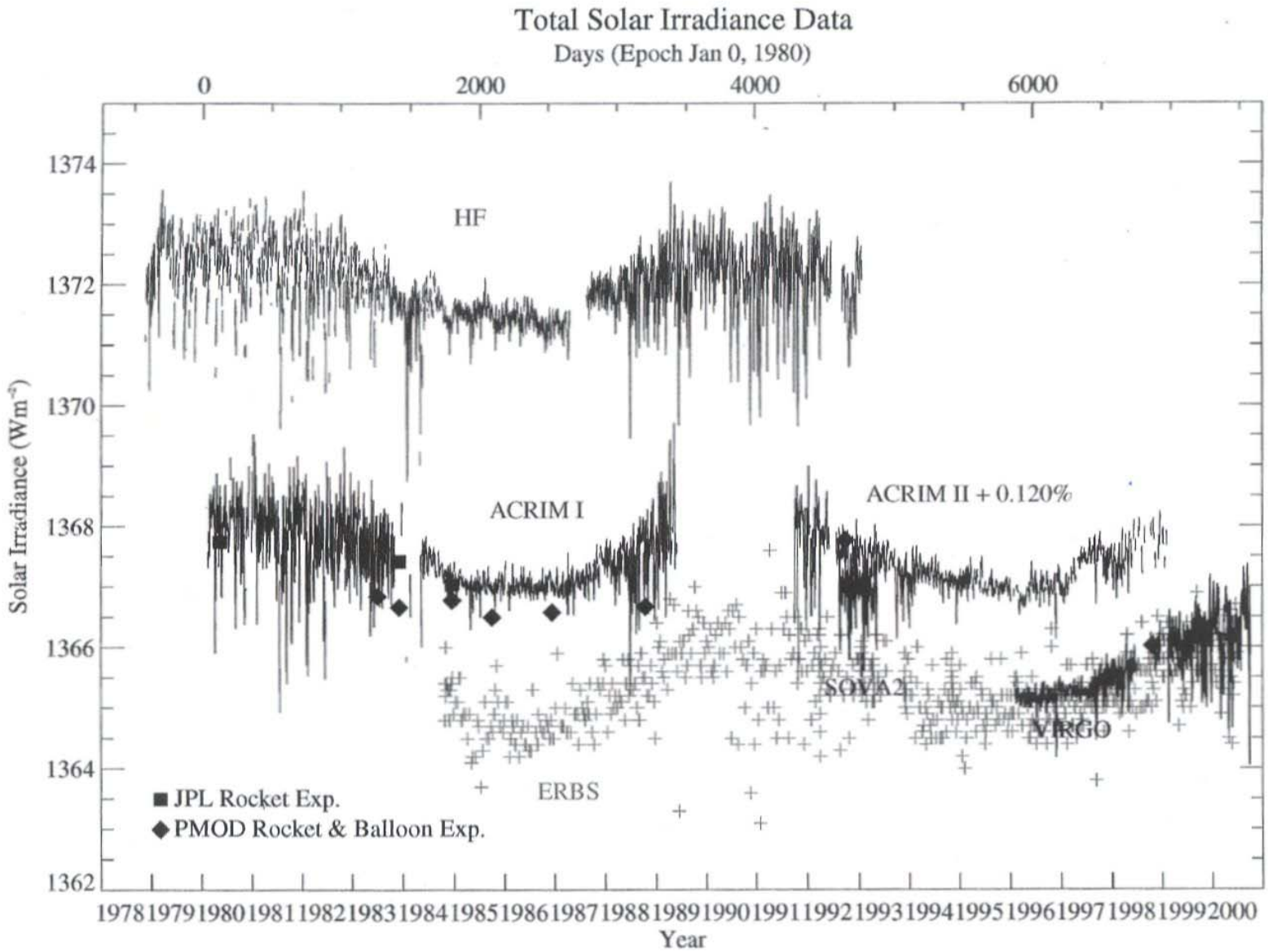

from: C. Fröhlich, Space Science Reviews, in preparation, and the VIRGO Team (Dec 03, 2000)

Frölich et al

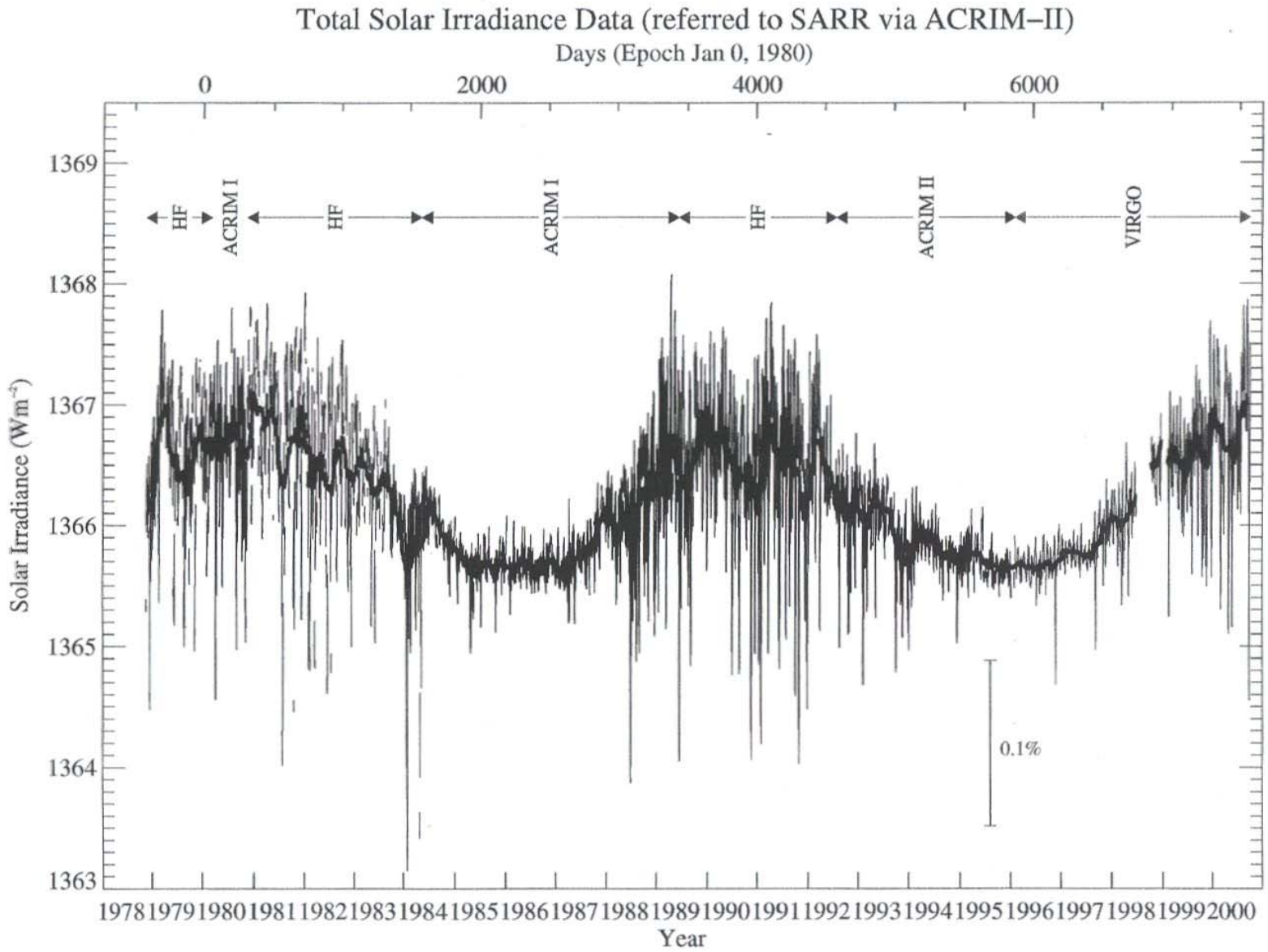

from: C. Fröhlich, Space Science Reviews, in preparation, and the VIRGO Team (Dec 03, 2000)

Fröhlich et al

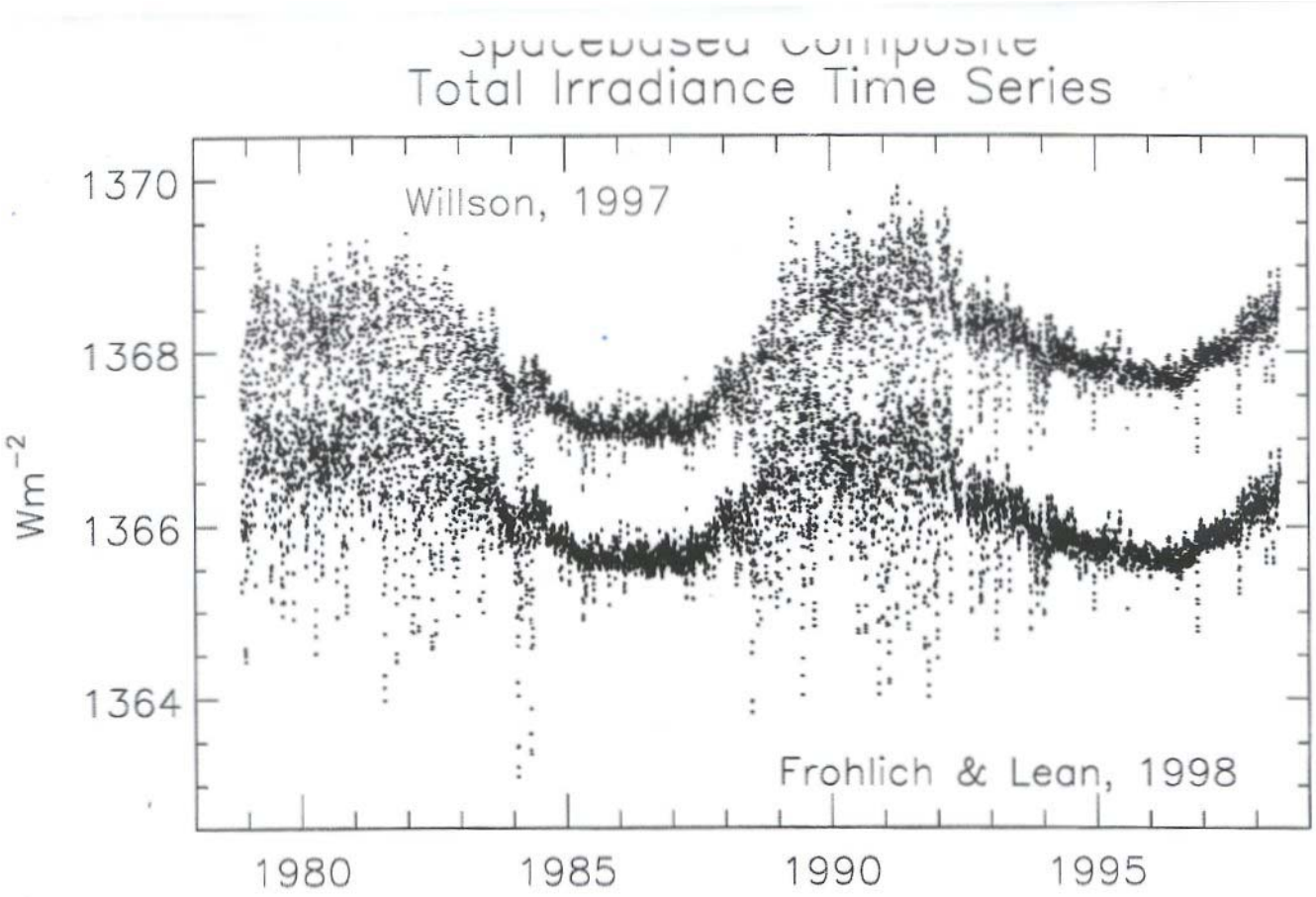

Fig. 6.10.2: Total solar irradiance composites derived from satellite data by Willson (1997) and Frohlich and Lean (1998).

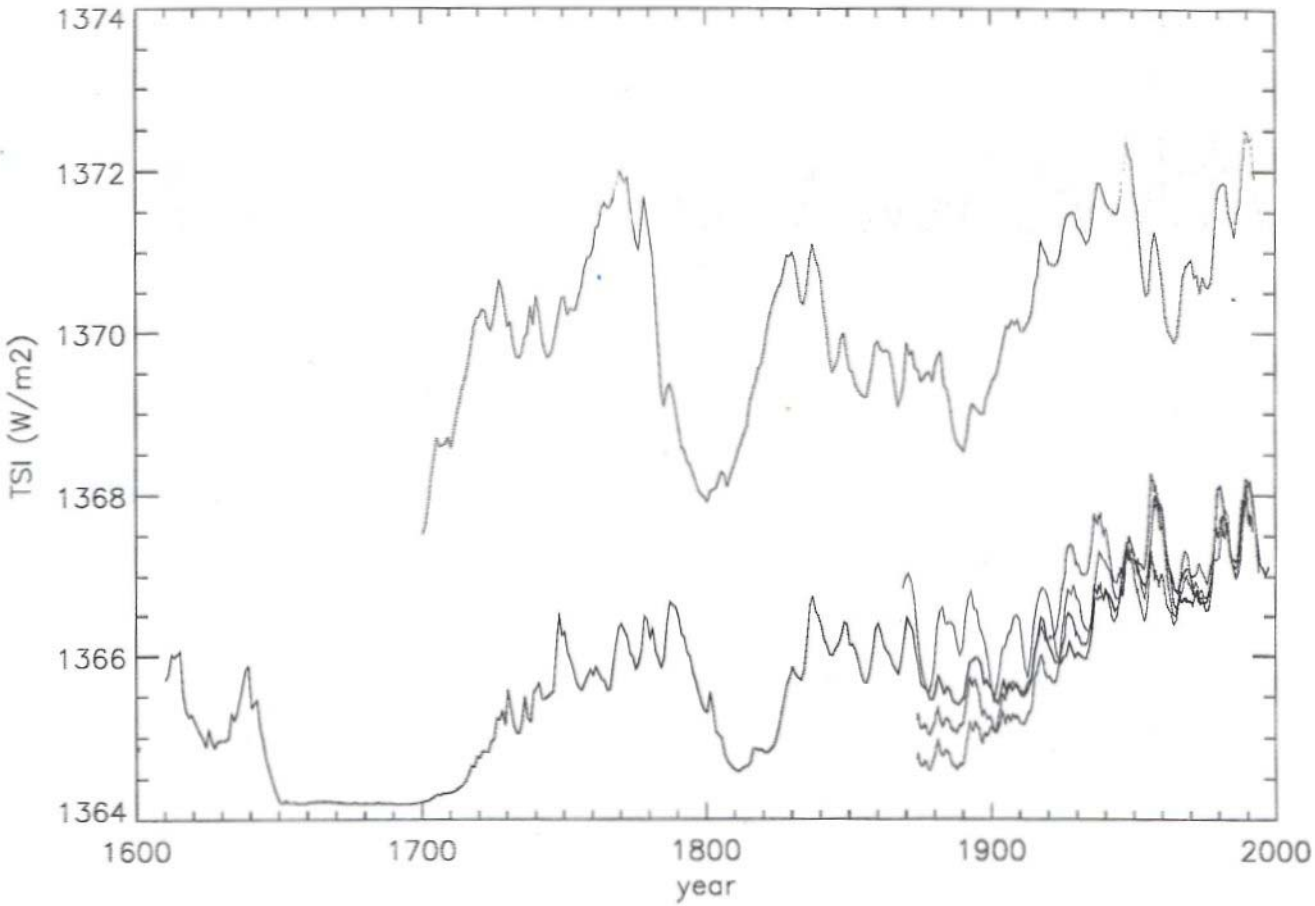

Fig. 6.10.3: Reconstructions of total solar irradiance by:
blue - Hoyt and Schatten (1993),
black - Lean, Beer and Bradley (1995),
cyan - Solanki and Fligge (1998) version A,
green - ditto version B,
red - Lockwood and Stamper (1999),
yellow - group sunspot numbers (Hoyt and Schatten, 1997) scaled to Nimbus-7 observations for 1979–1993.

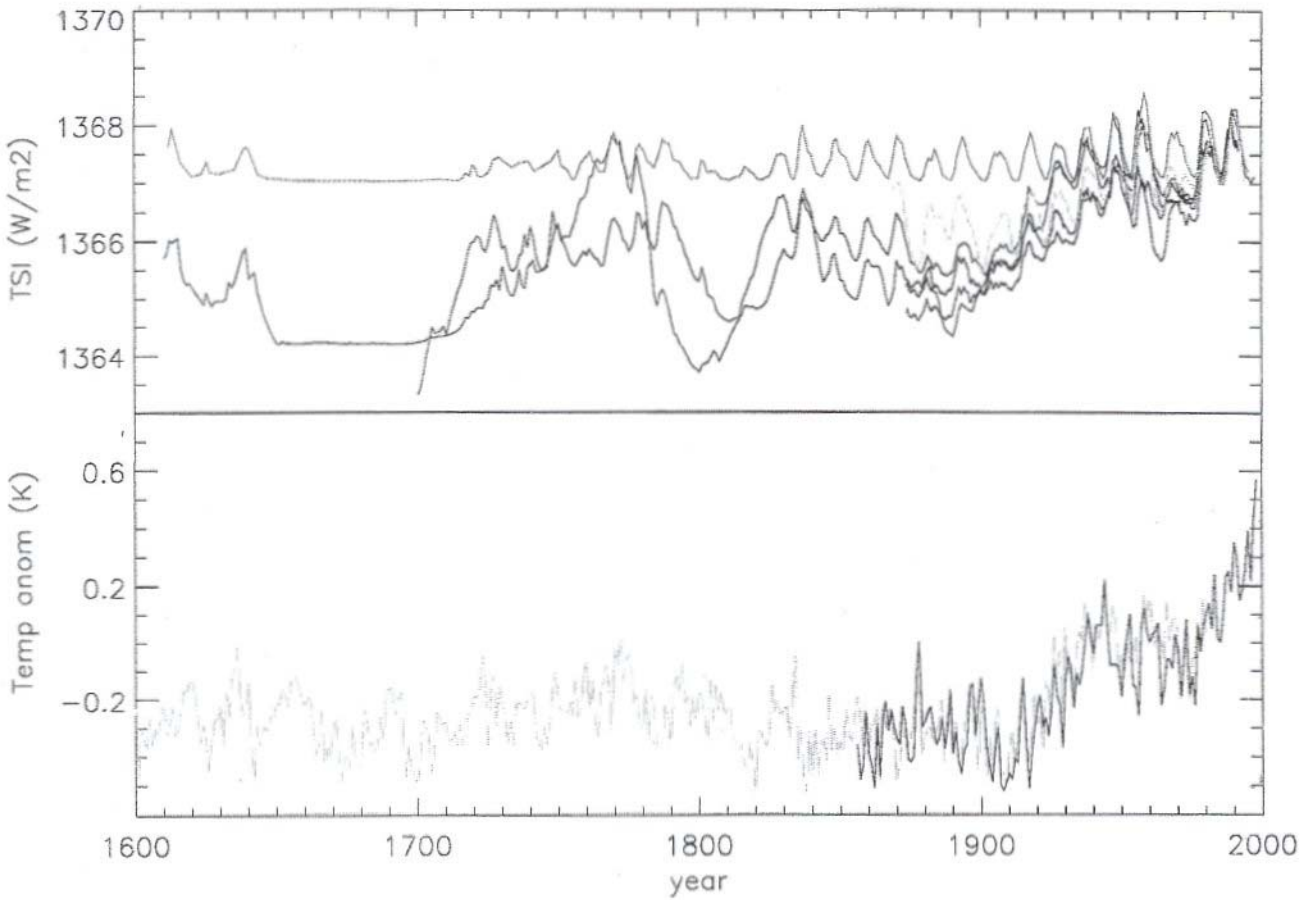
1370
1368
1366
1364
TSI (W/m2)
0.6
0.2
−0.2
Temp anom (K)
1600
1700
1800
1900
2000
year

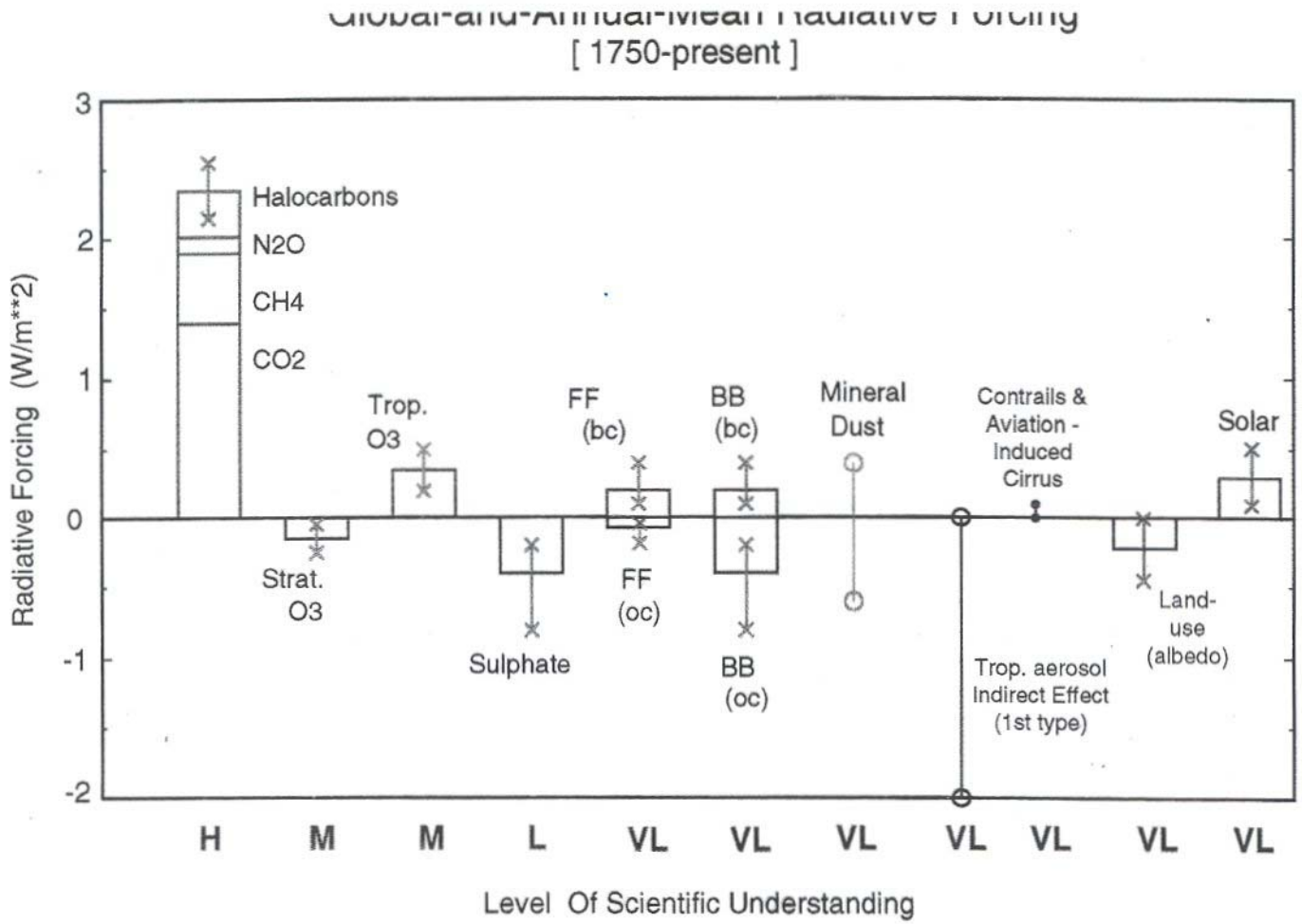

Fig. 6.13.1: Global, annual-mean radiative forcings (Wm^{-2}) due to a number of agents. The height of the bar denotes a "best gues" value. The vertical line about the bar indicates a range of likelihood of finding the actual estimate. The range is based on published estimates and additional knowledge concerning the processes leading to the forcing. A "level of scientific understanding" (LOSU) index is accorded to each forcing. This represents our subjective judgement involving factors such as the assumptions necessary to evaluate the forcing, the robustness of the physical mechanisms determining the forcing, and the uncertainties surrounding the processes involved in the forcing. "FF" denotes fossil-fuel burning while "BB" denotes biomass burning aerosol. Each of these is separated into the "black carbon" (bc) and "organc carbon" (oc) components. The LOSU is also separated into that for the bc and oc components.

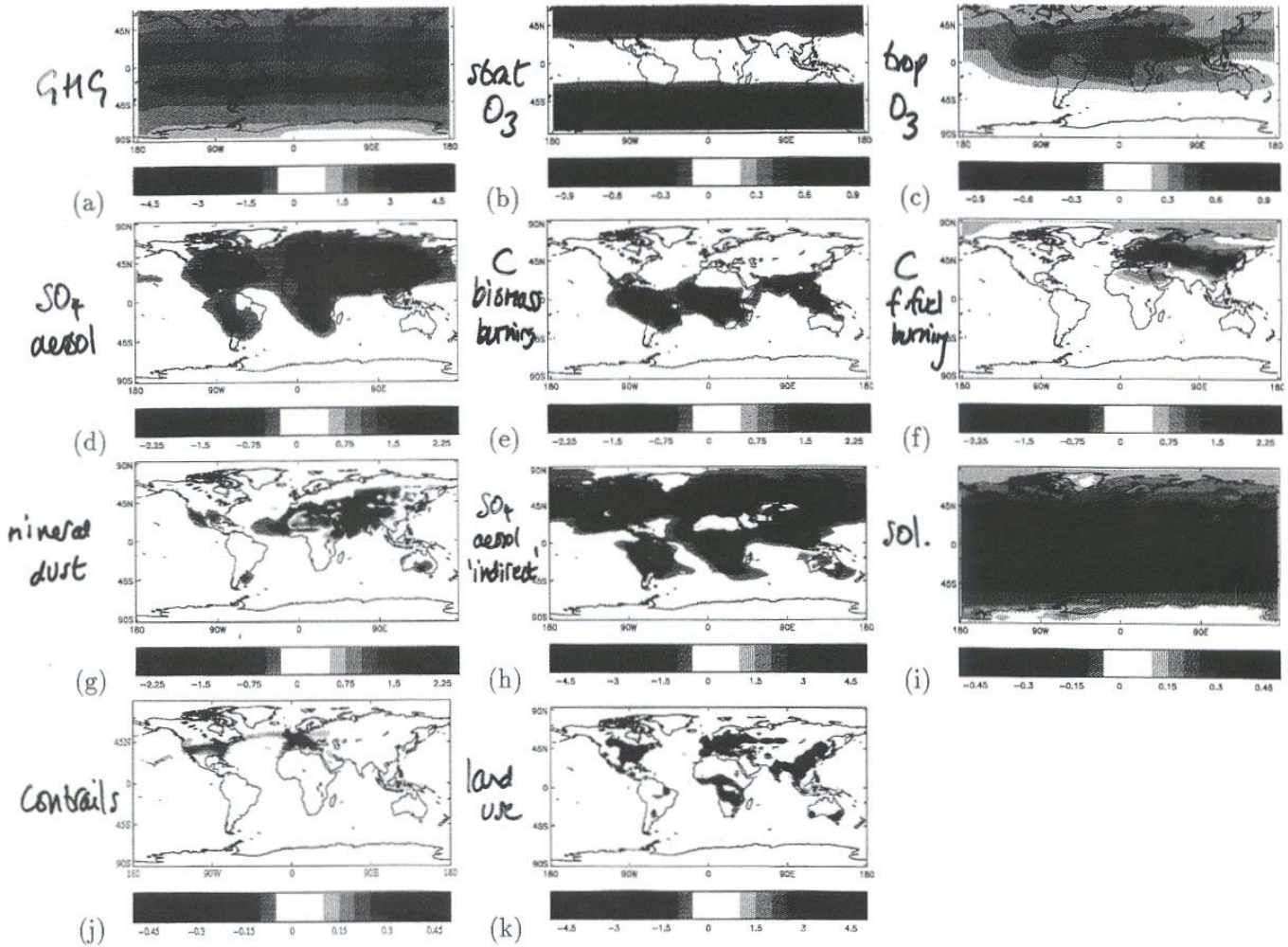

Fig. 6.14.1: Examples of the radiative forcing due to (a) well mixed greenhouse gases including carbon dioxide, methane, nitrous oxide, CFC-11 and CFC-12 (Shine and Forster, 1999); (b) stratospheric ozone depletion over the period 1979 to 1994 given by WMO, 1995 (Shine and Forster, 1999); (c) increases in tropospheric ozone (Berntsen *et al.*, 1997; Shine and Forster, 1999); (d) the direct effect of sulphate aerosol (Haywood *et al.*, 1997); (e) the direct effect of organic carbon and black carbon from biomass burning (Penner *et al.*, 1998; Grant *et al.*, 1999); (f) the direct effect of organic carbon and black carbon from fossil-fuel burning (Penner *et al.*, 1998; Grant *et al.*, 1999); (g) the direct effect of anthropogenic emissions of mineral dust (Tegen *et al.*, 1996); (h) the "first" indirect effect of sulphate aerosol (A. Jones, personal communication, 1999); (i) solar variability (Haigh, 1996); (j) contrails (Minnis *et al.*, 1999); (k) land use changes (Hansen *et al.*, 1998). Different modelling studies may show substantially different spatial patterns as described in the text.

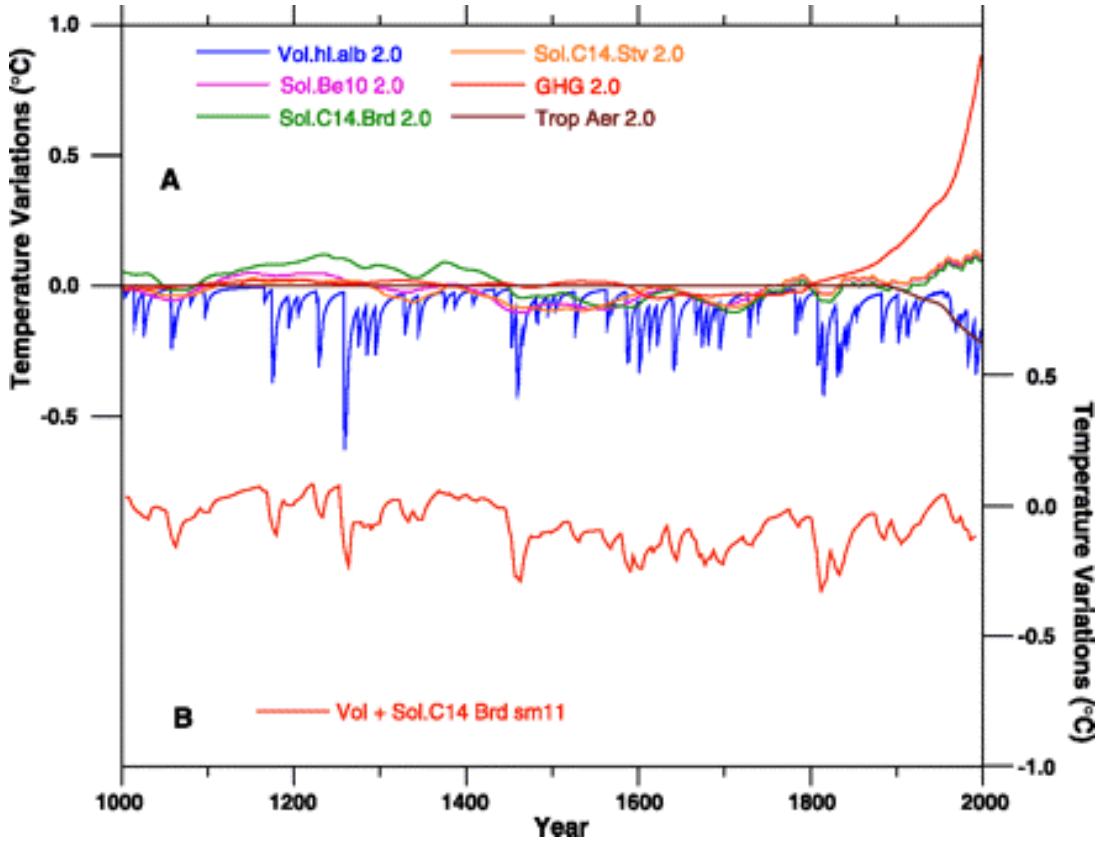
Vol.hl.alb 2.0
Sol.C14.Stv 2.0
Sol.Be10 2.0
GHG 2.0
Sol.C14.Brd 2.0
Trop Aer 2.0
A
B
Vol + Sol.C14 Brd sm11
Temperature Variations (°C)
Temperature Variations (°C)
Year
1.0
0.5
0.0
-0.5
-1.0
1000
1200
1400
1600
1800
2000

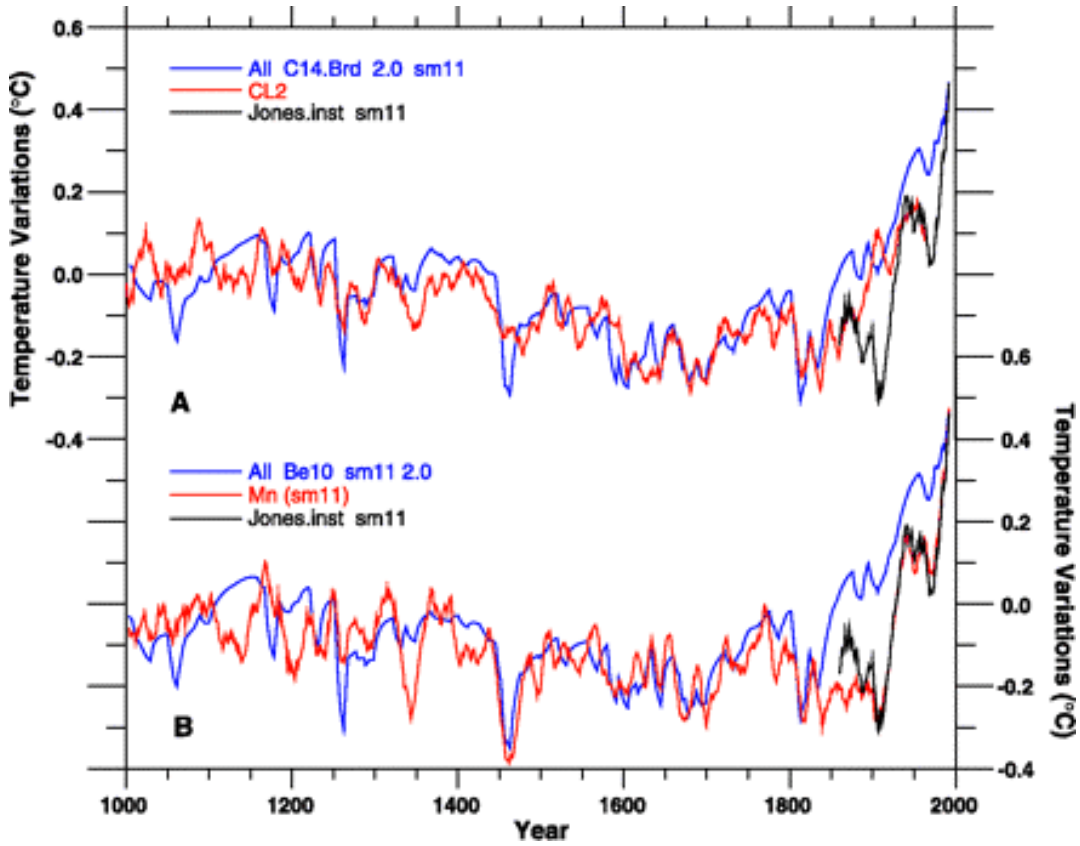
All C14.Brd 2.0 sm11
CL2
Jones.inst sm11
A
All Be10 sm11 2.0
Mn (sm11)
Jones.inst sm11
B
Temperature Variations (°C)
Temperature Variations (°C)
Year
0.6
0.4
0.2
0.0
-0.2
-0.4
1000
1200
1400
1600
1800
2000

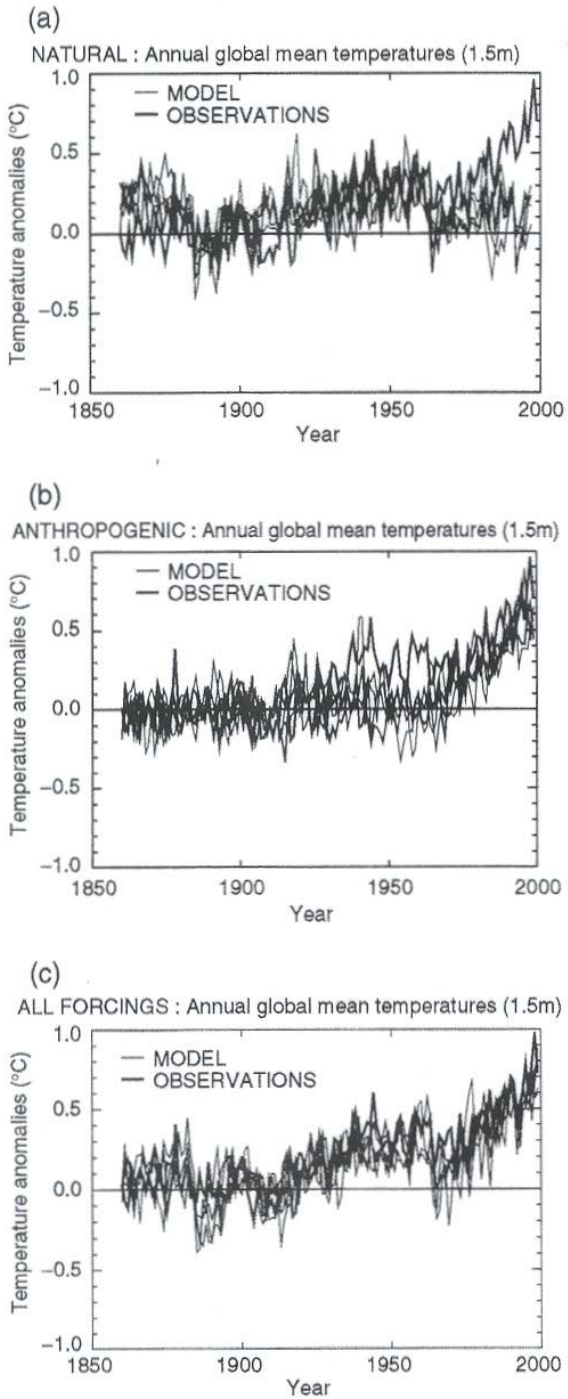

Figure 12.7: Global mean surface temperature anomalies relative to the 1880 to 1920 mean from the instrumental record compared with ensembles of four simulations with a coupled ocean-atmosphere climate model (from Stott *et al.*, 2000b; Tett *et al.*, 2000) forced (a) with solar and volcanic forcing only, (b) with anthropogenic forcing including well mixed greenhouse gases, changes in stratospheric and tropospheric ozone and the direct and indirect effects of sulphate aerosols, and (c) with all forcings, both natural and anthropogenic. The thick line shows the instrumental data while the thin lines show the individual model simulations in the ensemble of four members. Note that the data are annual mean values. The model data are only sampled at the locations where there are observations. The changes in sulphate aerosol are calculated interactively, and changes in tropospheric ozone were calculated offline using a chemical transport model. Changes in cloud brightness (the first indirect effect of sulphate aerosols) were calculated by an offline simulation (Jones *et al.*, 1999) and included in the model. The changes in stratospheric ozone were based on observations. The volcanic forcing was based on the data of Sato *et al.* (1993) and the solar forcing on Lean *et al.* (1995), updated to 1997. The net anthropogenic forcing at 1990 was 1.0 Wm^{-2} including a net cooling of 1.0 Wm^{-2} due to sulphate aerosols. The net natural forcing for 1990 relative to 1860 was 0.5 Wm^{-2}, and for 1992 was a net cooling of 2.0 Wm^{-2} due to Mt. Pinatubo. Other models forced with anthropogenic forcing give similar results to those shown in b (see Chapter 8, Section 8.6.1, Figure 8.15; Hasselmann *et al.*, 1995; Mitchell *et al.*, 1995b; Haywood *et al.*, 1997; Boer *et al.*, 2000a; Knutson *et al.*, 2000).

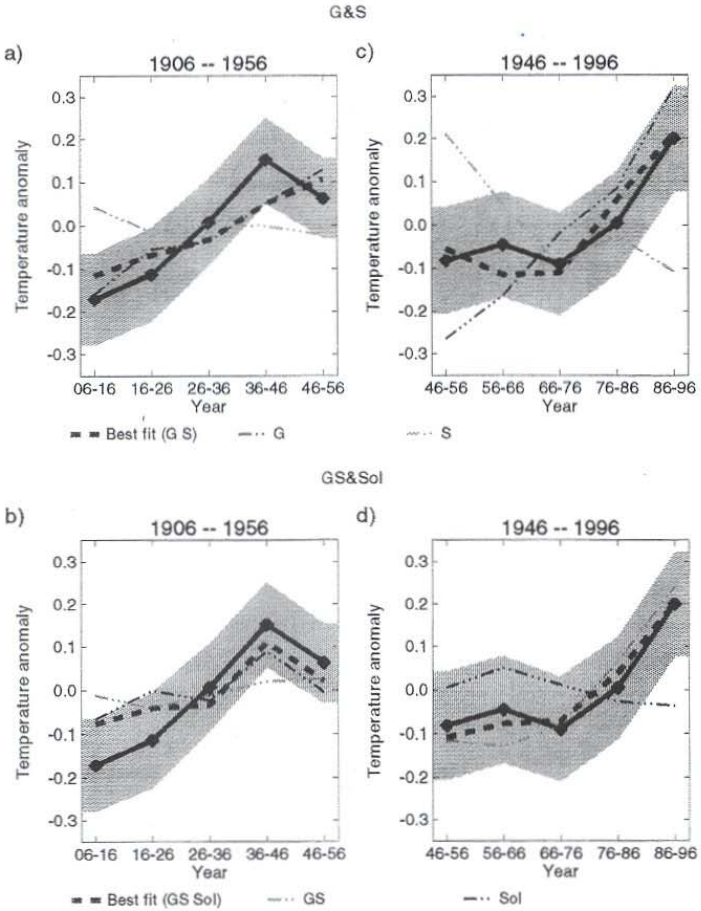

Figure 12.11: Best-estimate contributions to global mean temperature change. Reconstruction of temperature variations for 1906 to 1956 (a and b) and 1946 to 1995 (c and d) for G and S (a and c) and GS and SOL (b and d). (G denotes the estimated greenhouse gas signal, S the estimated sulphate aerosol signal, GS the greenhouse gas / aerosol signal obtained from simulations with combined forcing, SOL the solar signal). Observed (thick black), best fit (dark grey dashed), and the uncertainty range due to internal variability (grey shading) are shown in all plots. (b) and (d) show contributions from GS (orange) and SOL (blue). (a) and (c) show contributions from G (red) and S (green). All time-series were reconstructed with data in which the 50-year mean had first been removed. (Tett *et al.*, 1999).

errors are persistent over time. An example based on the IS92a (IPCC, 1992) GS scenario (whose exact forcing varies between models, see Chapter 9, Table 9.1 for details) is shown in Figure 12.13 based on a limited number of model simulations. Note that in each case, the original warming predicted by the model lies in the range consistent with the observations. A rate of warming of 0.1 to 0.2°C/decade is likely over the first few decades of the 21st century under this scenario. Allen *et al.* (2000b) quote a 5 to 95% ("very likely") uncertainty range of 0.11 to 0.24°C/decade for the decades 1996 to 2046 under the IS92a scenario, but, given the uncertainties and assumptions behind their analysis, the more cautious "likely" qualifier is used here. For comparison, the simple model tuned to the results of seven AOGCMs used for projections in Chapter 9 gives a range of 0.12 to 0.22°C/decade under the IS92a scenario, although it should be noted that this similarity may reflect some cancellation of errors and equally good agreement between the two approaches should not be expected for all scenarios, nor for time-scales longer than the few decades for which the Allen *et al.* (2000b) approach is valid. Figure 12.13 also shows that a similar range of uncertainty is obtained if the greenhouse gas and sulphate components are estimated separately, in which case the estimate of future warming for this particular scenario is independent of possible errors in the amplitude of the sulphate forcing and response. Most of the recent emission scenarios indicate that future sulphate emissions will decrease rather than increase in the near future. This would lead to a larger global warming since the greenhouse gas component would no longer be reduced by sulphate forcing at the same rate as in the past. The level of uncertainty also increases (see Allen *et al.*, 2000b). The final error bar in Figure 12.13 shows that including the model-simulated response to natural forcing over the 20th century into the analysis has little impact on the estimated anthropogenic warming in the 21st century.

It must be stressed that the approach illustrated in Figure 12.13 only addresses the issue of uncertainty in the large-scale climate response to a particular scenario of future greenhouse gas

Stott et al (2001, Clim. Dyn. submitted)

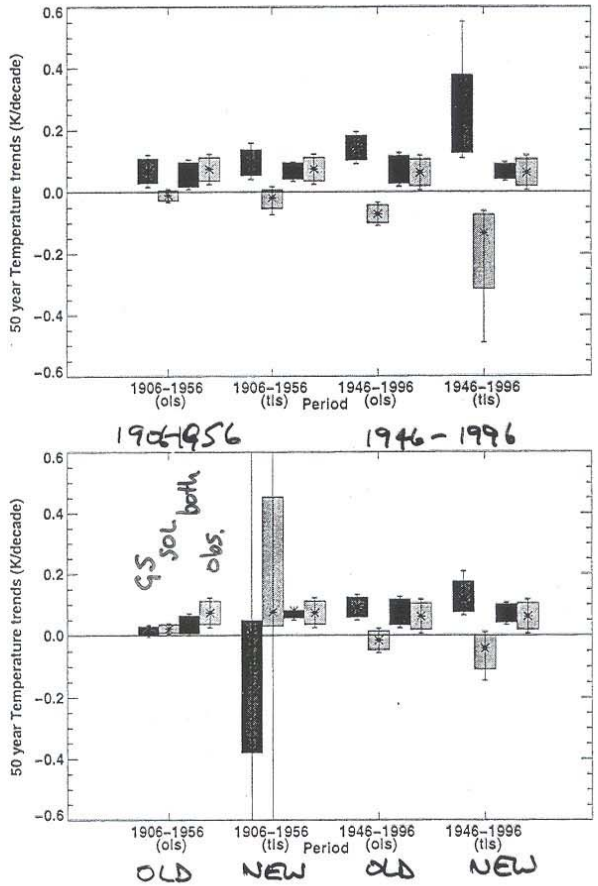

Figure 4: a)50-year global mean temperature trends and uncertainties as reconstructed using OLS and TLS regression for the 1906-56 and the 1946-96 periods. For each 50-year period 4 bars represent the 10-90 percentiles and 4 lines represent the 5-95 percentiles of, respectively, from left : temperature trends due to **GHG**, **SUL**, the combined trends from both and the observed trends. Best estimates are shown as stars. b) as (a) where 4 bars and 4 lines represent respectively, from left : **GS**, **Sol**, combined trends from both and the observed trends.

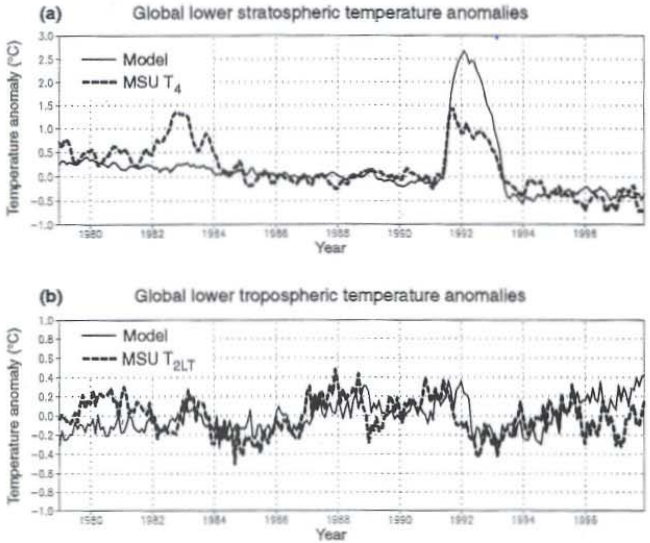

Figure 12.4: (a) Observed microwave sounding unit (MSU) global mean temperature in the lower stratosphere, shown as dashed line, for channel 4 for the period 1979 to 97 compared with the average of several atmosphere-ocean GCM simulations starting with different atmospheric conditions in 1979 (solid line). The simulations have been forced with increasing greenhouse gases, direct and indirect forcing by sulphate aerosols and tropospheric ozone forcing, and Mt. Pinatubo volcanic aerosol and stratospheric ozone variations. The model simulation does not include volcanic forcing due to El Chichon in 1982, so it does not show stratospheric warming then. (b) As for (a), except for 2LT temperature retrievals in the lower troposphere. Note the steady response in the stratosphere, apart from the volcanic warm periods, and the large variability in the lower troposphere (from Bengtsson *et al.*, 1999).

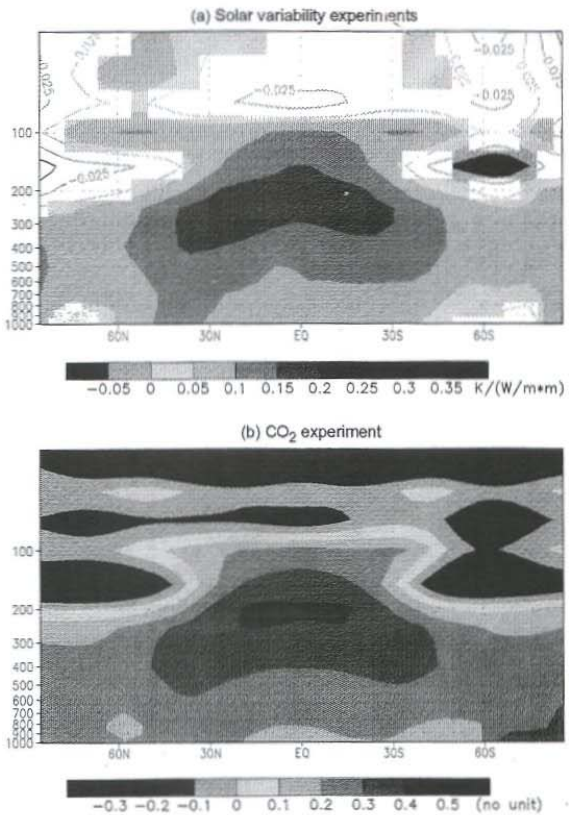

Figure 12.5: (a) Response (covariance, normalised by the variance of radiance fluctuations) of zonally averaged annual mean atmospheric temperature to solar forcing for two simulations with ECHAM3/LSG. Coloured regions indicate locally significant response to solar forcing. (b) Zonal mean of the first EOF of greenhouse gas-induced temperature change simulated with the same model (from Cubasch *et al.*, 1997). This indicates that for ECHAM3/LSG, the zonal mean temperature response to greenhouse gas and solar forcing are quite different in the stratosphere but similar in the troposphere.

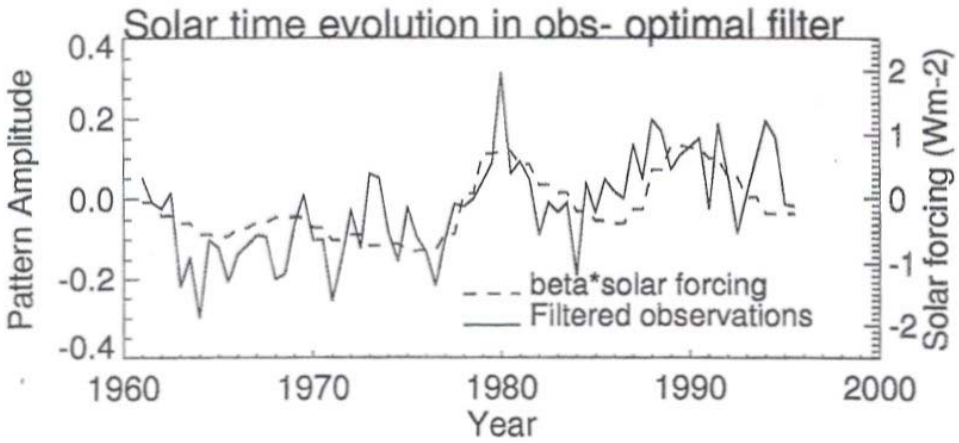

Figure 8: Filtered observations and solar forcing for optimal fingerprint filter.

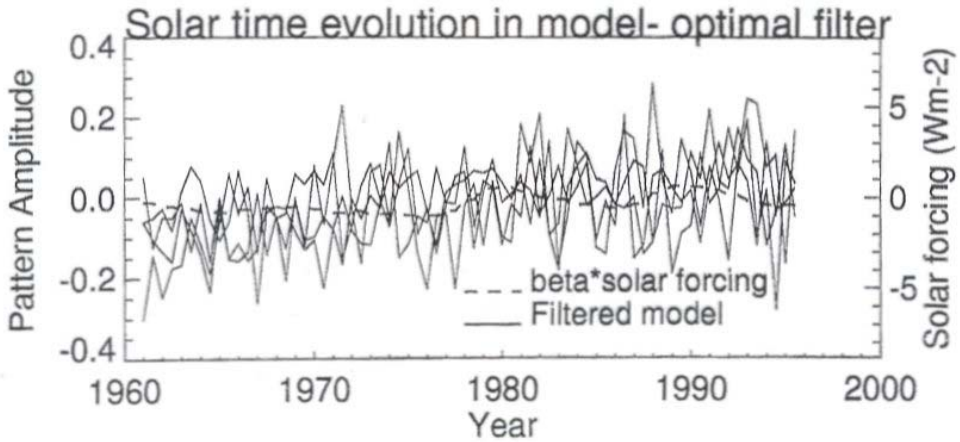

Figure 9: Filtered model ensemble members and solar forcing for optimal fingerprint filter.

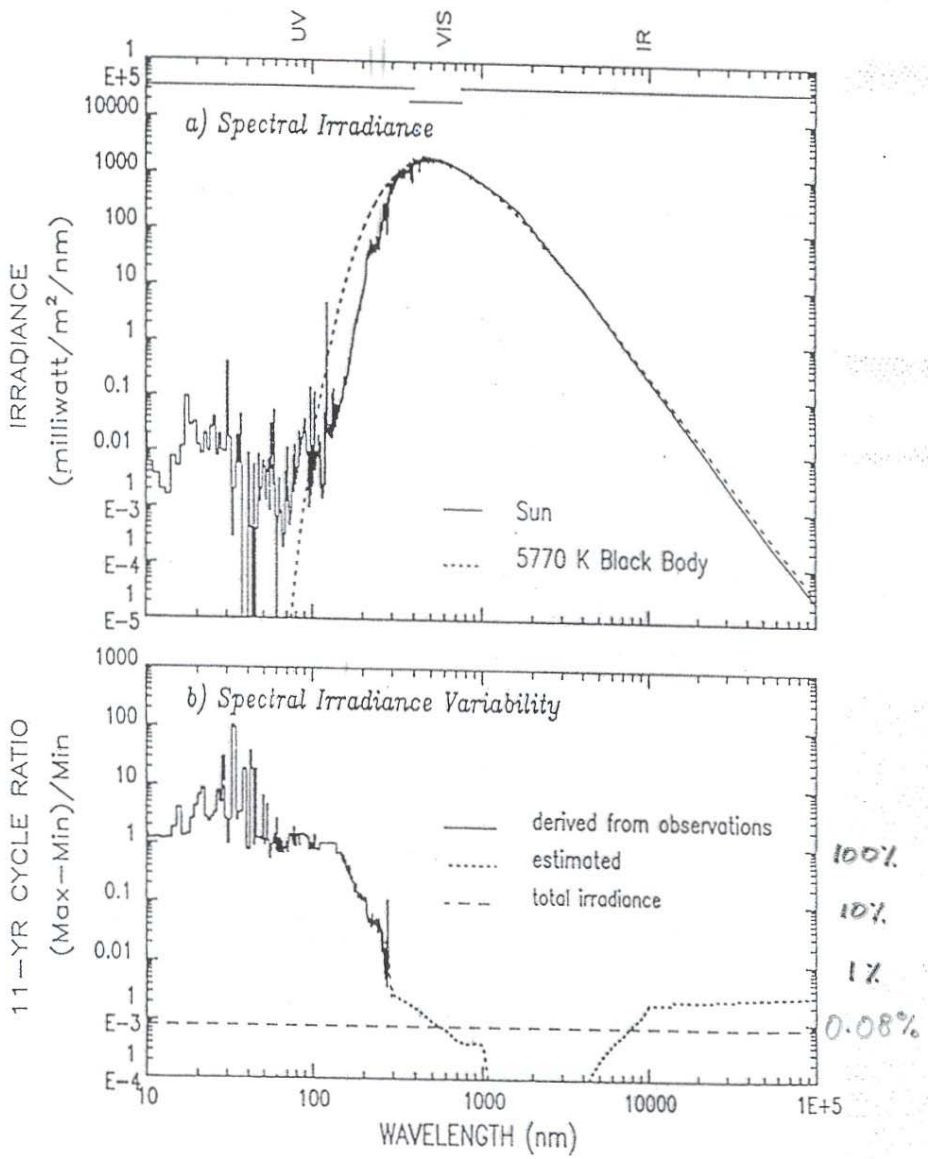
UV
VIS
IR
a) Spectral Irradiance
IRRADIANCE
(milliwatt/m²/nm)
Sun
5770 K Black Body
b) Spectral Irradiance Variability
11-YR CYCLE RATIO
(Max-Min)/Min
derived from observations
estimated
total irradiance
100%
10%
1%
0.08%
WAVELENGTH (nm)

Kodera JGR 1773

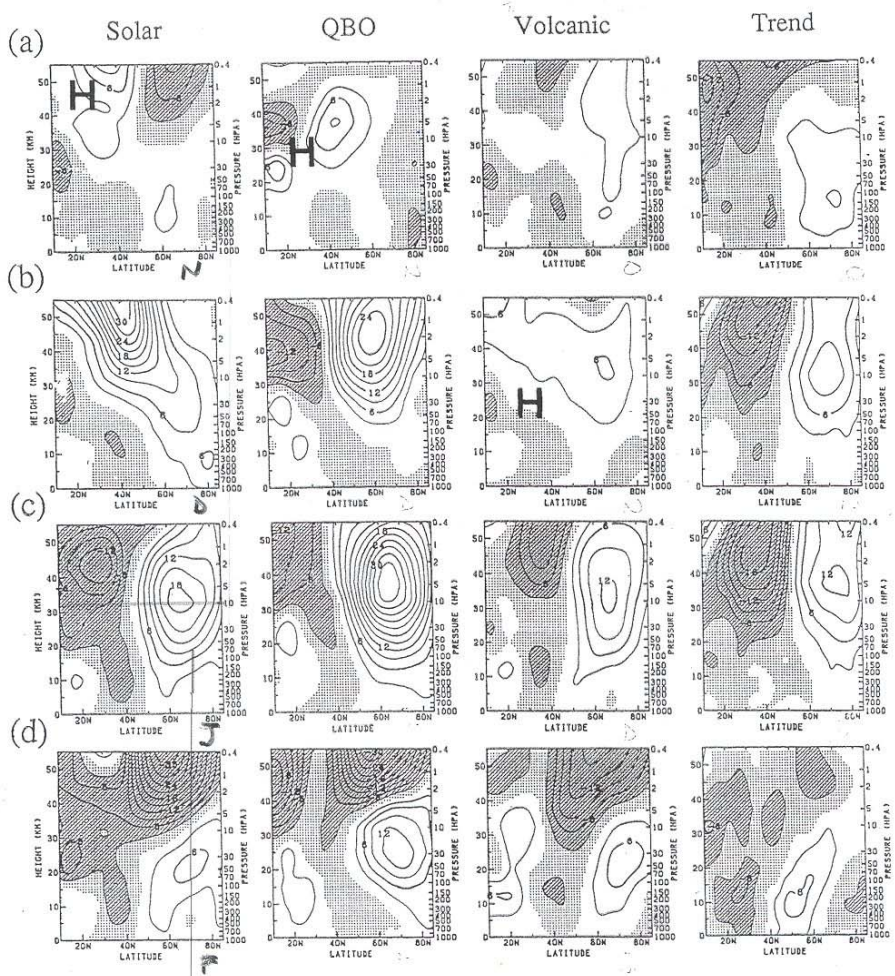

Figure 1. Meridional cross sections of the monthly mean anomalous zonal-mean zonal wind composed for (from left to right) the solar, QBO, volcanic, and trend cases during fall to winter (from November to February for the solar and QBO cases, but October to January for the volcanic and trend cases). See text for details. The contour interval is 3 ms^{-1}, and zero line suppressed. Negative values are stippled and values smaller than -3 ms^{-1} are shaded.

the thermal wind relationship. Figure 3 shows composite means of meridional temperature gradient for the solar, QBO, volcanic, and trend cases, from left to right. Unlike Figure 1, they are equally arranged from top to bottom according to the calendar month from November to January. In November (Figure 3, top), to the north of the possible heating region, indicated by H as in Figure 1, a negative temperature gradient (warmer toward the equator or cooler toward the north pole) is found. These negative anomalies near the northern end of the possible source regions develop downward and poleward from December, and large negative anomalies are commonly found in the polar regions of the lower stratosphere in January. Diverse patterns found in November become similar in January with negative anomalies in the polar region of the lower stratosphere and positive anomalies in the stratopause regions. In the troposphere, as negative anomalies develop in the polar region, positive anomalies grow in a rather limited area around 40°N, 500 hPa. (This last one is, in fact, related to the tropospheric warming at midlatitudes as can be found in Figure 1 of *Kodera* [1994].)

Unlike the zonal winds case, the anomalous temperature gradients initially found near the possible source regions

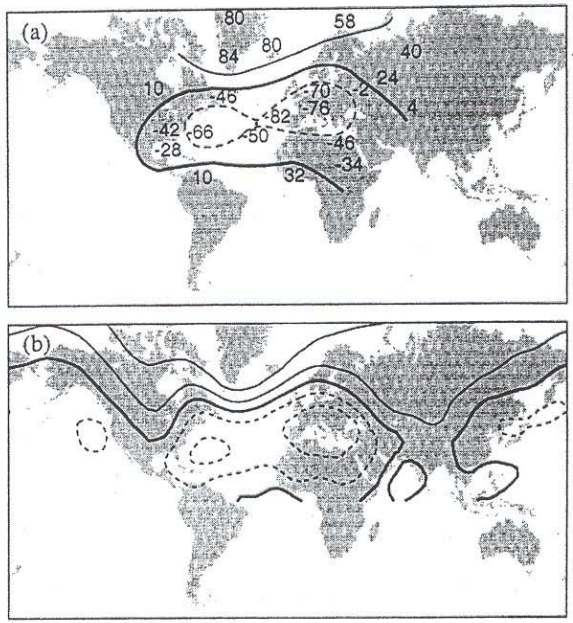

Figure 1. Correlation maps for December to February seasonal-mean sea-level pressure (SLP) based on the North Atlantic Oscillation (NAO) of Walker and Bliss (1932). (a) A reproduction of chart 2 from their paper: contour interval 60. (b) The same analysis for 1950–94 based on gridded United Kingdom Meteorological Office SLP (Basnett and Parker 1997). See text for further details. Contour interval 30, negative contours are dashed, and the zero contour is bold.

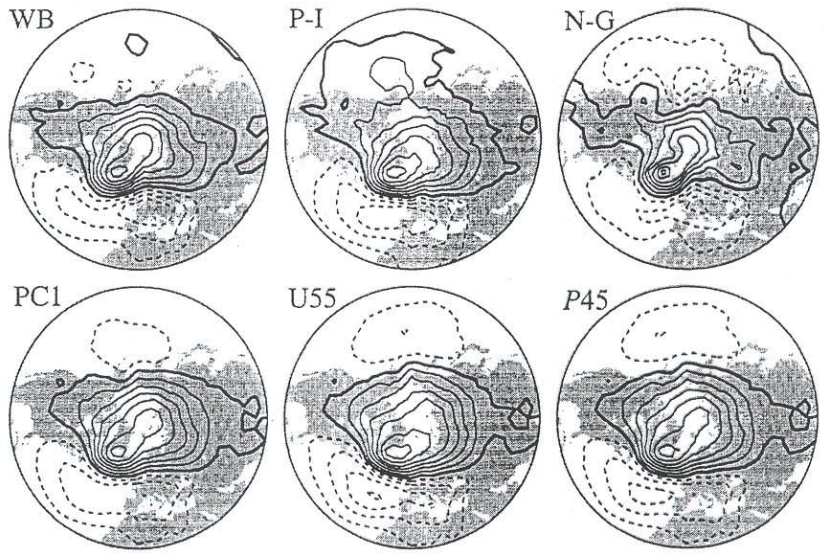

Figure 2. Correlation maps for the indices listed in Table 2 based on (upper panels) seasonal-mean and (lower panels) monthly December–March United Kingdom Meteorological Office sea-level pressure data (Basnett and Parker 1997) for the period of record 1950–94. Contour interval 0.15, negative contours are dashed, and the zero

Geopotential anomalies

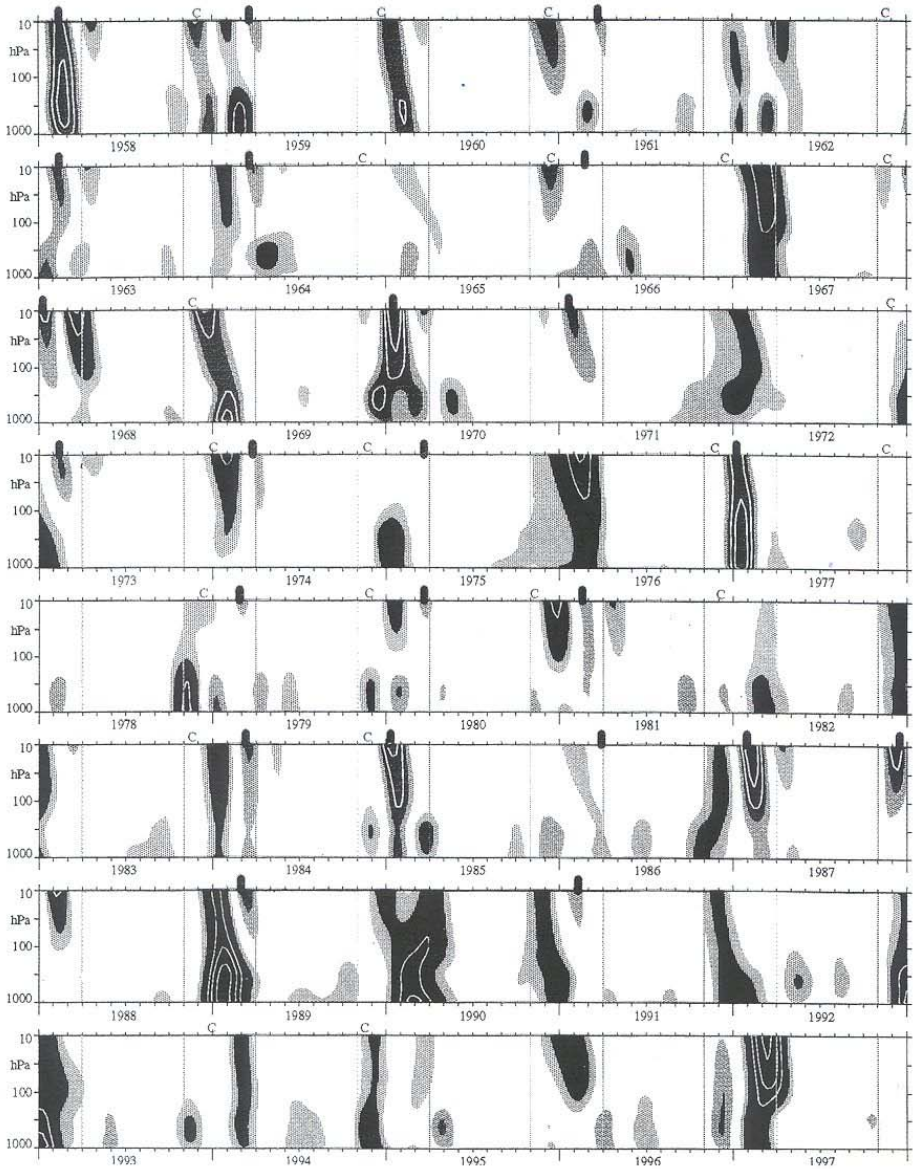

Baldwin & Dunkerton (JGR 1999)

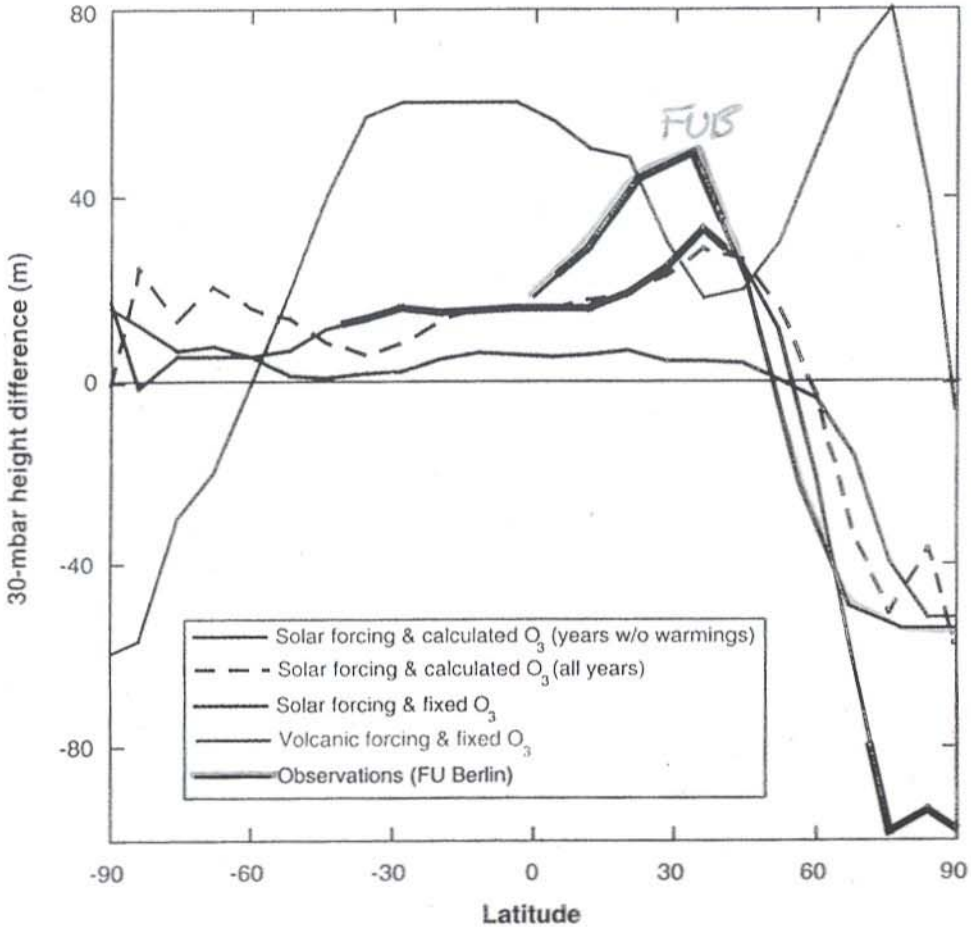

Fig. 1. Modeled zonal mean differences in December–February 30-mbar geopotential heights between solar maximum and solar minimum in GISS GCM runs with interactive ozone, both for the entire simulation and for only those years without sudden warmings (*23*), and with constant ozone. Also shown are results from a simulation with Pinatubo-like volcanic forcing (*24*). In that simulation, sea surface temperatures were allowed to adjust, so the results are taken from only the first 3 years (a rough lifetime for volcanic aerosols injected into the stratosphere). Thick portions of lines indicate statistical significance (>90%) for the interactive ozone run and for 40 years of observations (*2*). In the region where the observations are statistically significant, the results from the calculated ozone experiment are within the uncertainty of the observations for both analyses.

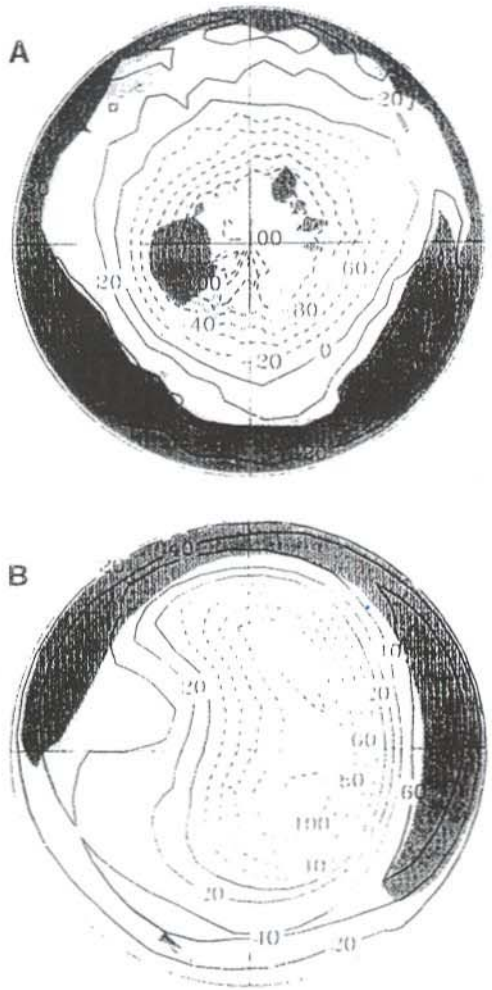

Fig. 2. December–February 30-mbar geopotential height differences between solar maximum and solar minimum for years without stratospheric warmings (**A**), and in the observations (as in Fig. 1) (**B**) (*2*). The shading shows 90% (light) and 95% (dark) significance levels.

Shindell et al

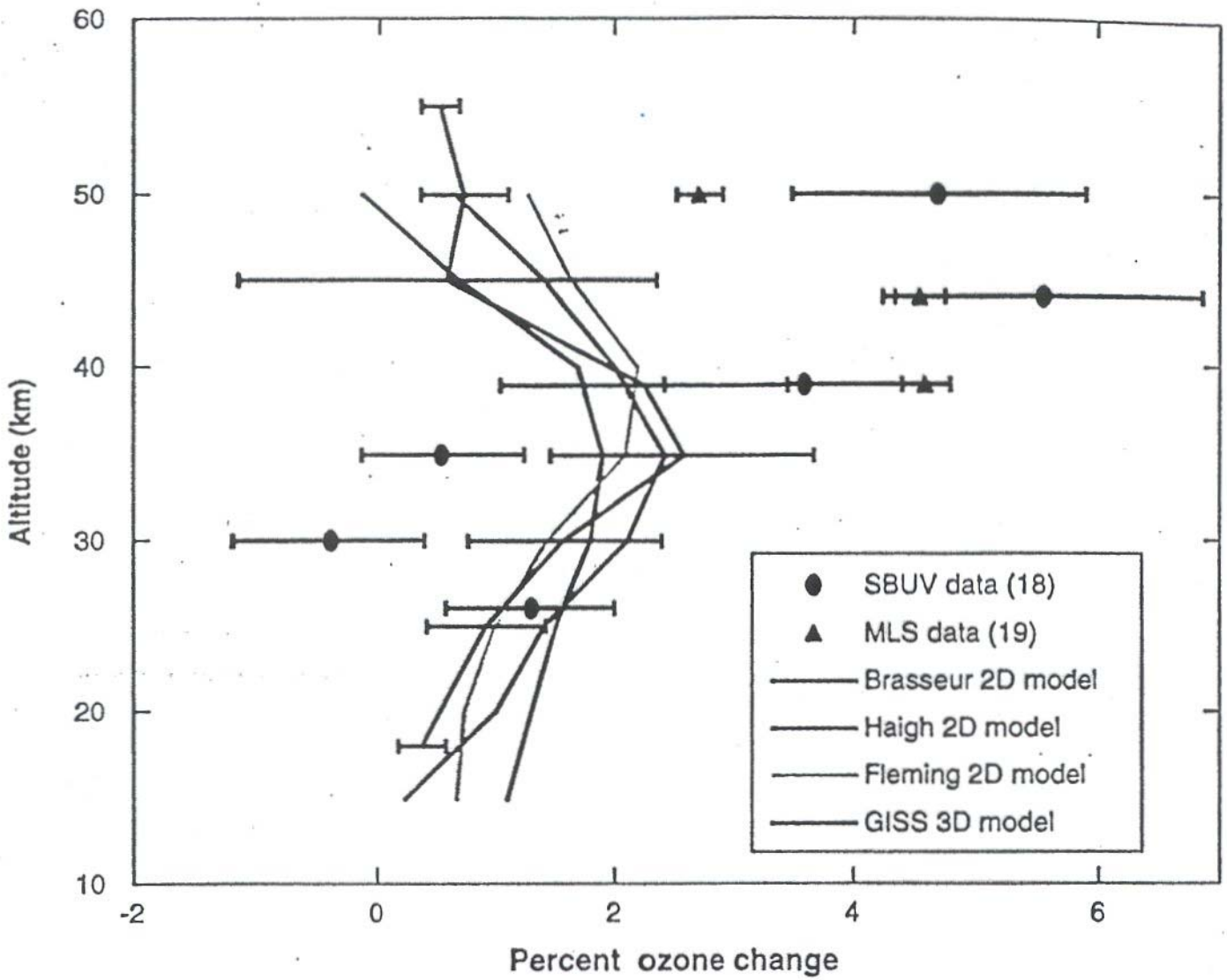

Fig. 3. Annual average percentage ozone differences between solar maximum and solar minimum averaged from 60°S to 60°N. The data points are from satellite observations covering 15 years for Solar Backscatter Ultraviolet (SBUV) data (*18*) and 3 years for Microwave Limb Sounder (MLS) data (*19*). The lines give results from the indicated models, including ozone-temperature feedbacks. GISS results are from the GCM, including our 2D model–derived parameterizations of ozone photochemistry.

ΔO_3 (%)

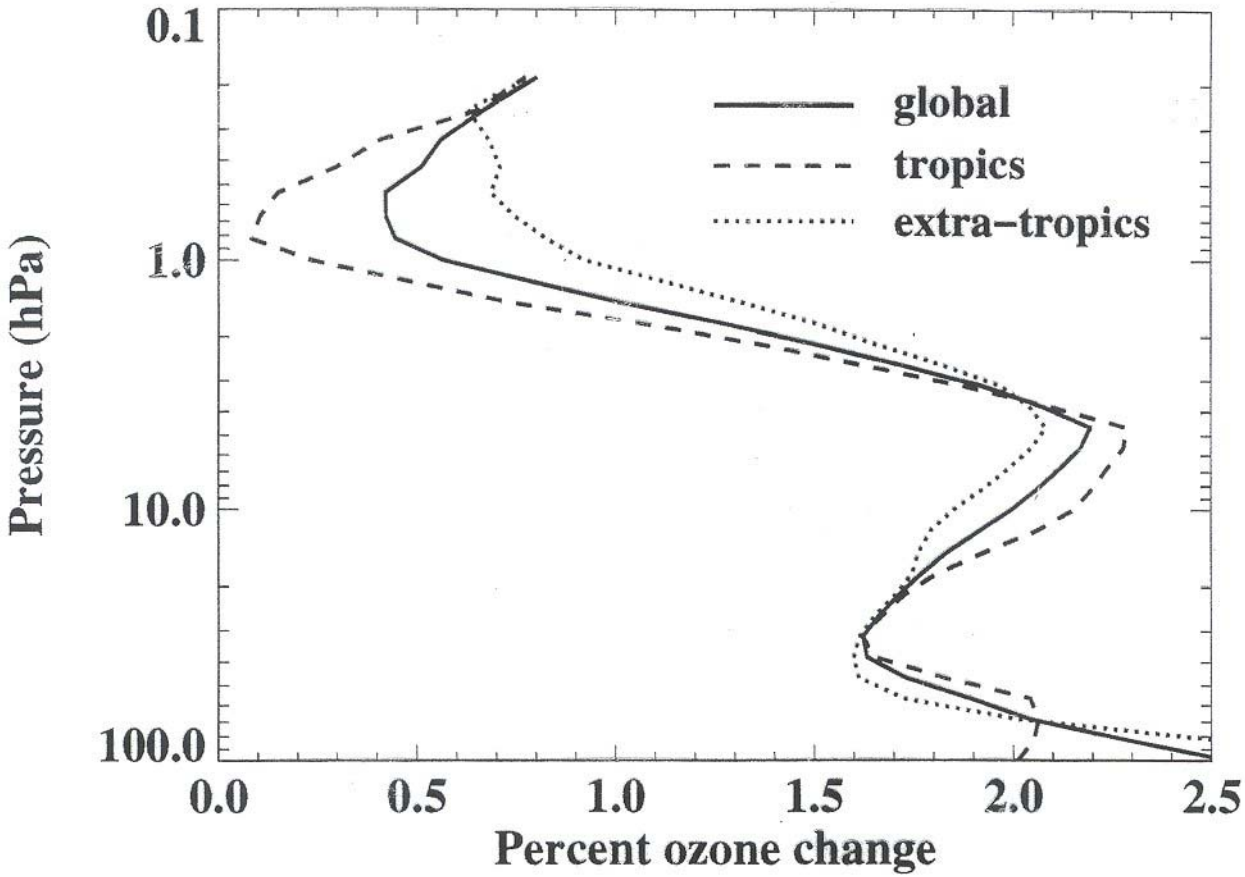
0.1
1.0
10.0
100.0
Pressure (hPa)
0.0
0.5
1.0
1.5
2.0
2.5
Percent ozone change
global
tropics
extra–tropics

Conclusions

Solar variability makes an important contribution to decadal-to-century scale climate variability.

GCMs possibly underestimate climate response to solar variability.

Mechanisms whereby the direct impact of changes in total solar irradiance may be amplified are not well established but may include:

- Changes to thermal structure of the stratosphere affecting planetary wave propagation in the winter hemisphere.
- Changes to the equatorial lower stratosphere affecting the tropical Hadley cells.

The effect of solar variability on stratospheric ozone is not well established.

Shortwave Heating Rates at Solar Minimum and Differences Between Solar Maximum and Minimum for 4 Maximum Scenario
(6 Band Resolution)

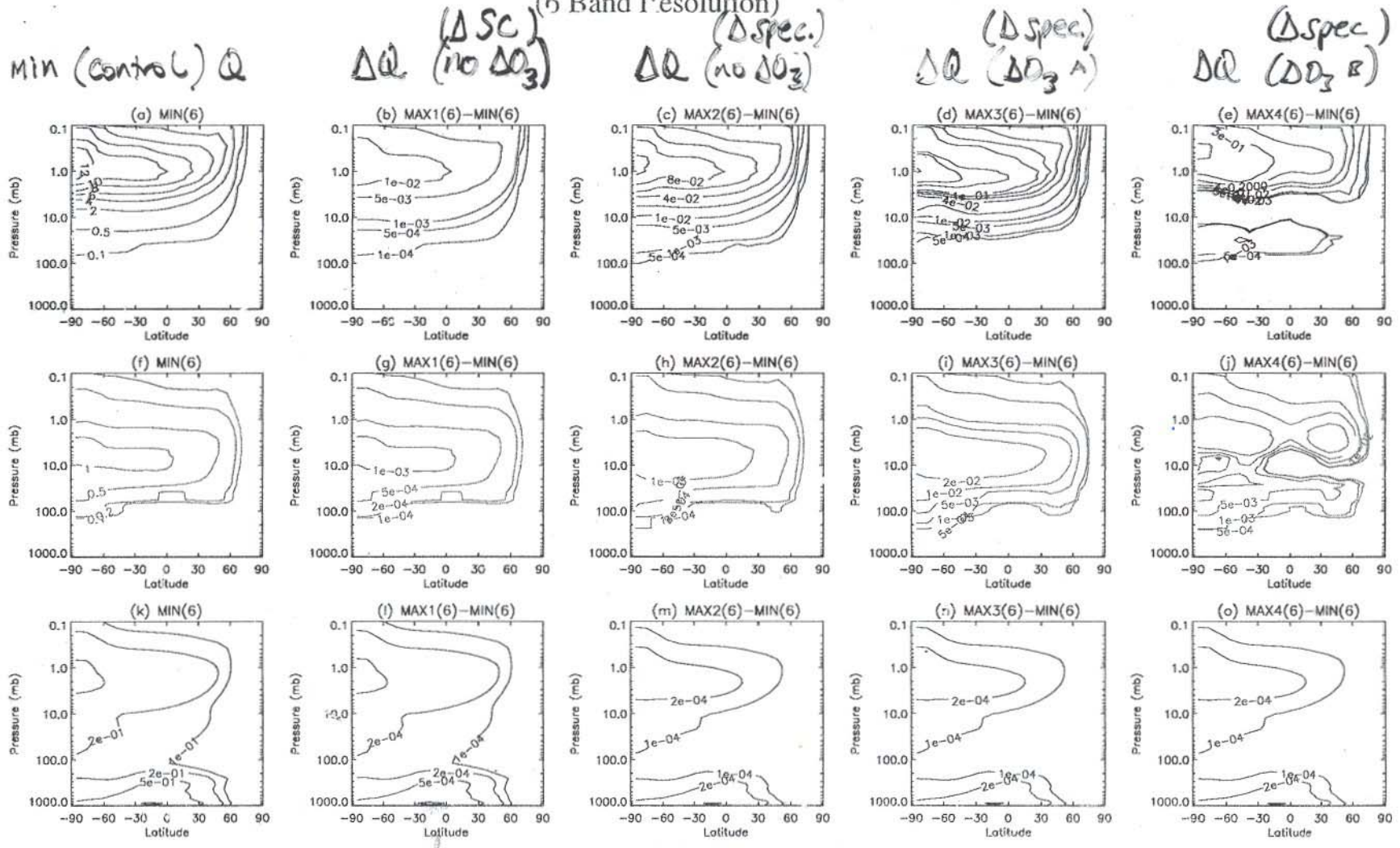

Plots for January over height and latitude, (a) UV at solar minimum, (b) – (e) difference between solar maximum and solar minimum for 4 different scenarios in the UV region, (f) VIS at solar minimum, (g) – (j) as (b) to (e) but for VIS, (k) IR at solar minimum, (l) - (o), as (b) to (e) but for IR.

Larkin, Haigh & Djavidnia (2000)

Change in clear sky downward irradiance at 100 hPa ($W M^{-2}$)

Solar max.

— solar min.

——— no ΔO_3

..... 2D ΔO_3

- - - - - TOMS ΔO_3

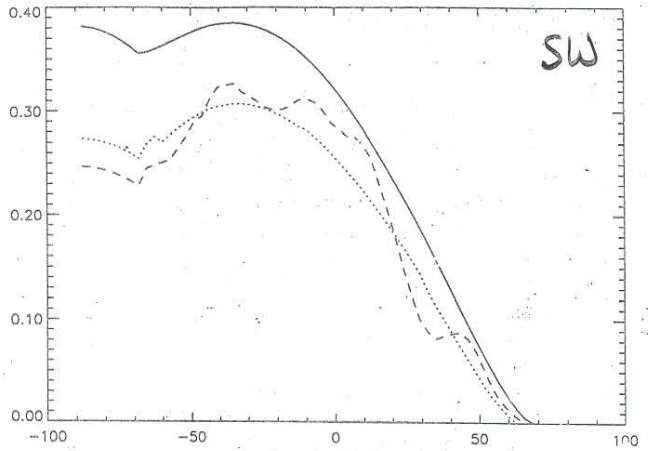

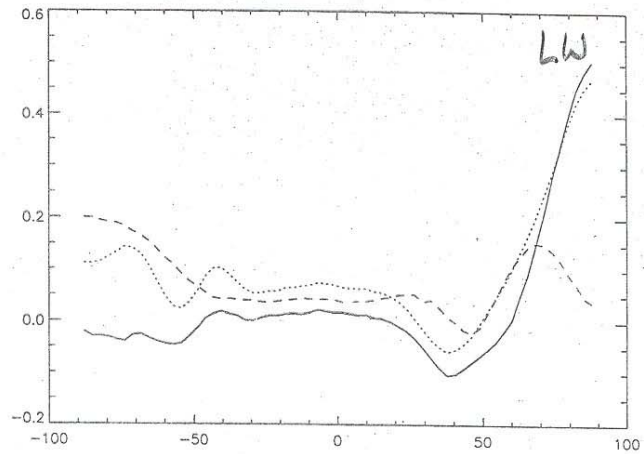

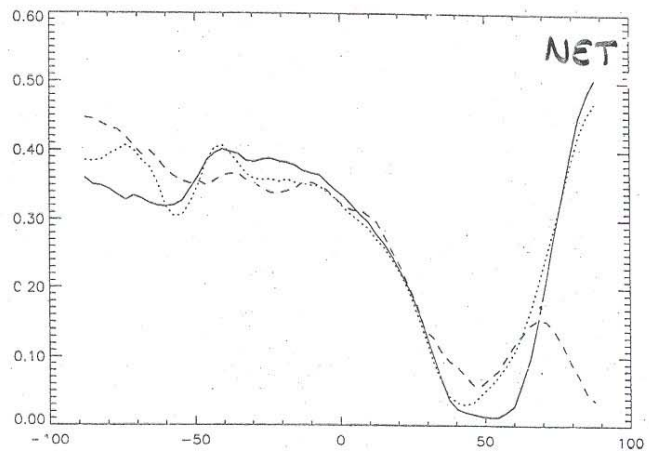

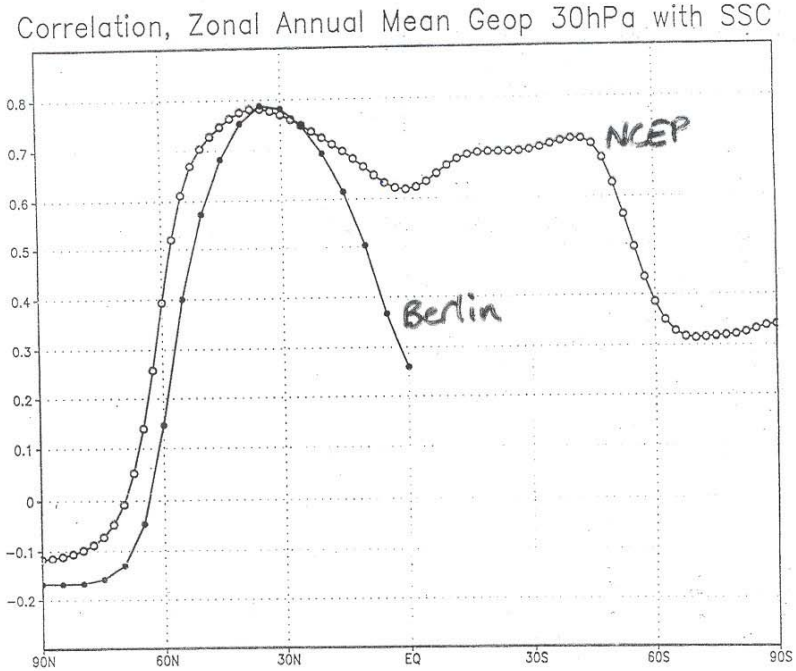

Labitzke & van Loon 1997

UGCM

ΔZ_{30} (m)

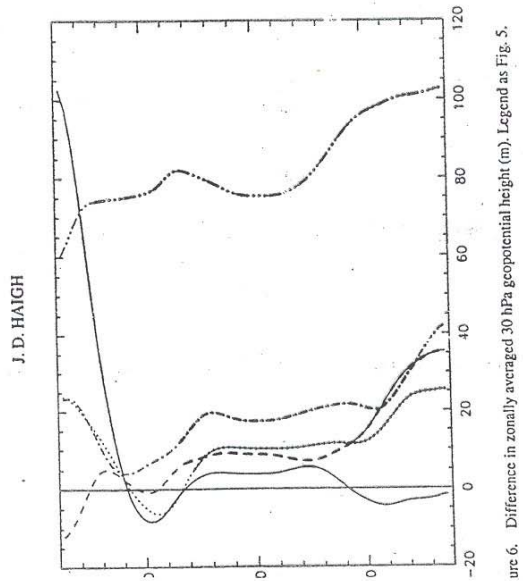

ure 6. Difference in zonally averaged 30 hPa geopotential height (m). Legend as Fig. 5.

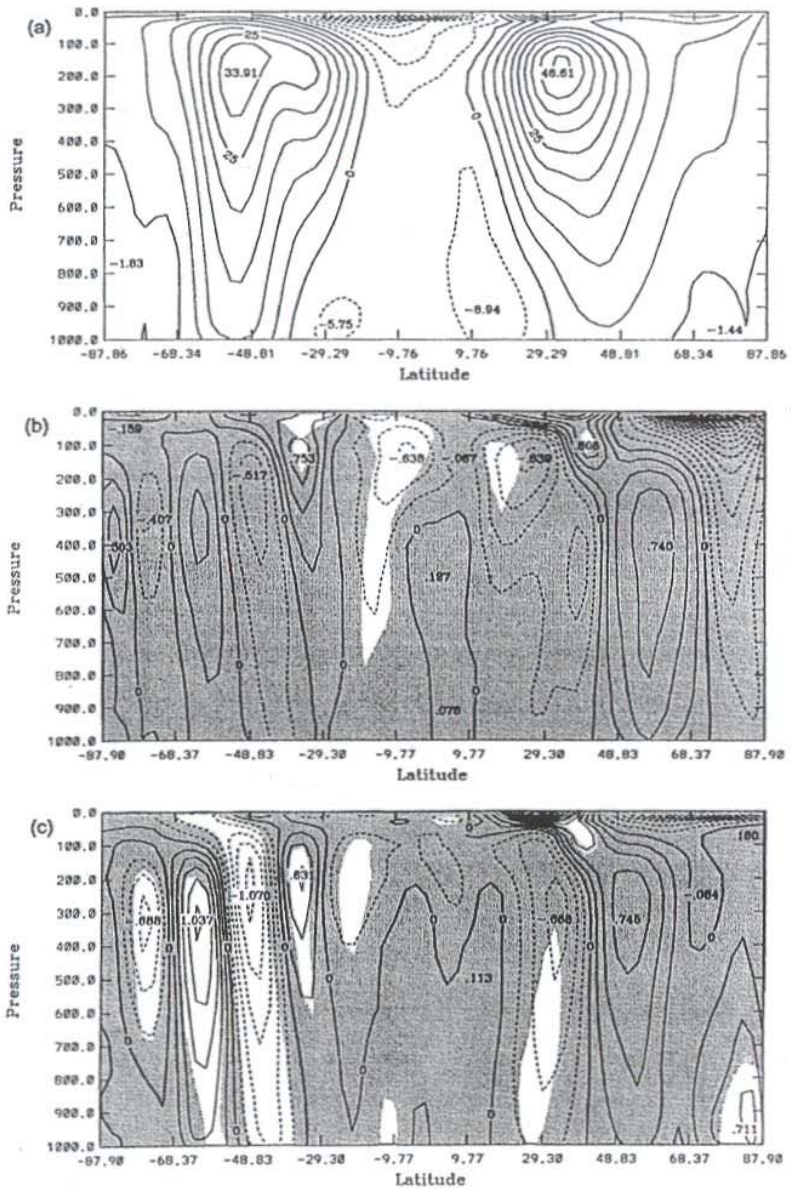

Figure 3. As Fig. 2 but for zonal-mean zonal wind (m s^{-1}).

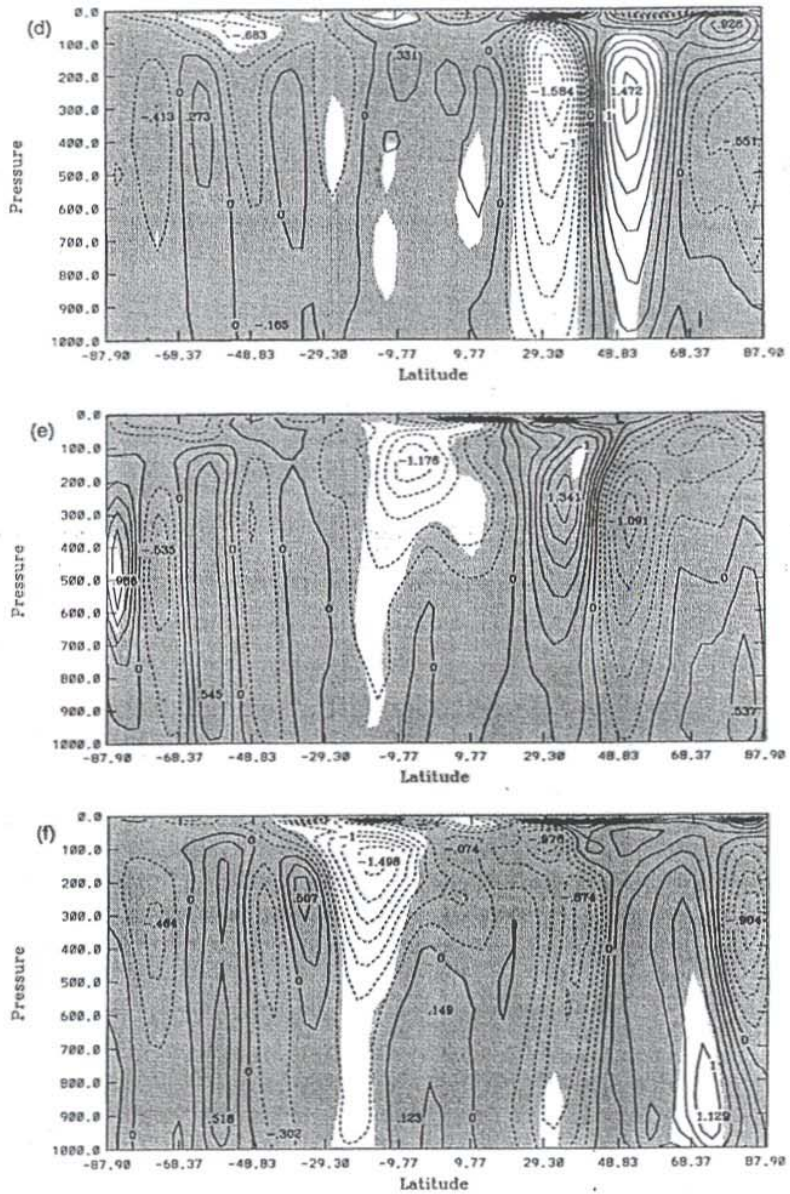

Figure 3. Continued.

Jan

$\bar{u}$ (MS^{-1})

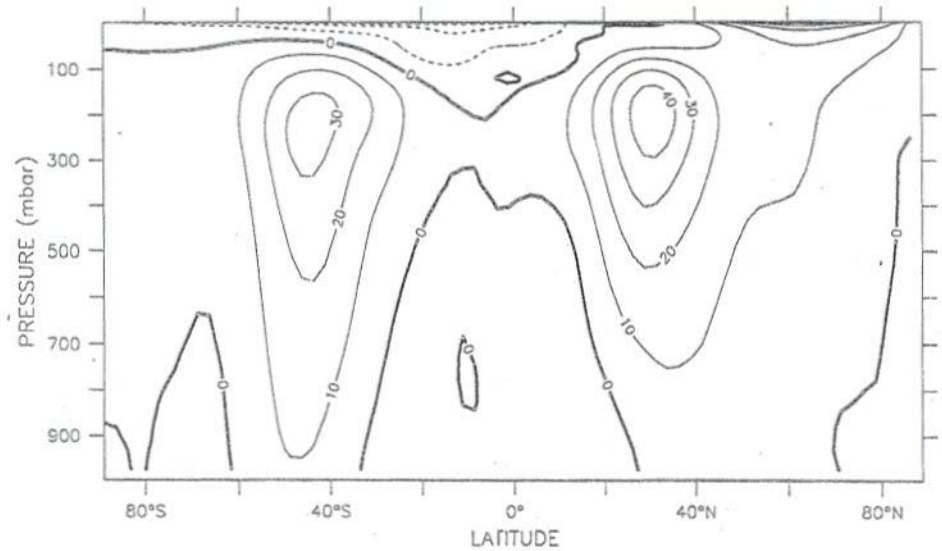

$\Delta\bar{u}$

EXP 1

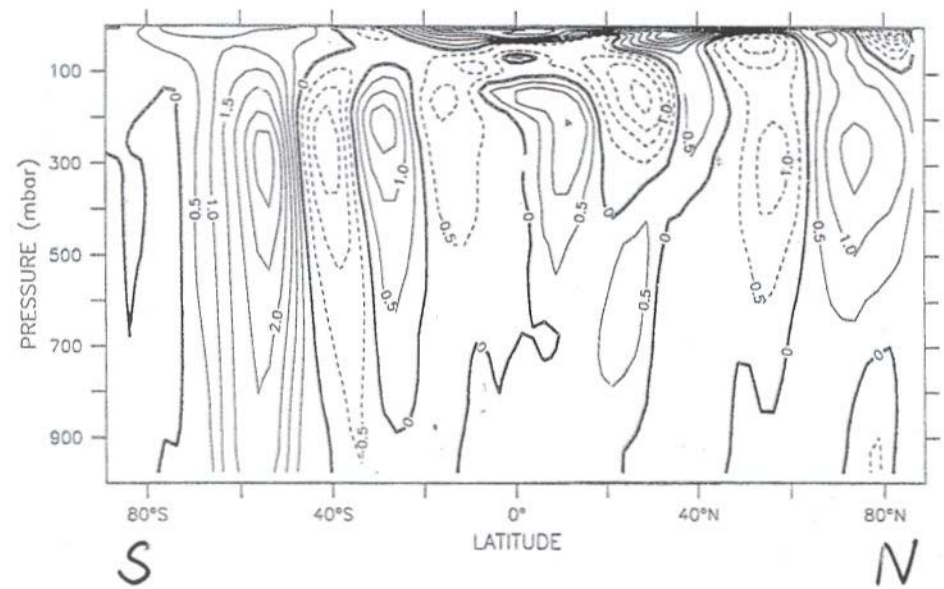

NCEP ū 1979–1991 regression coefficients

SOLAR

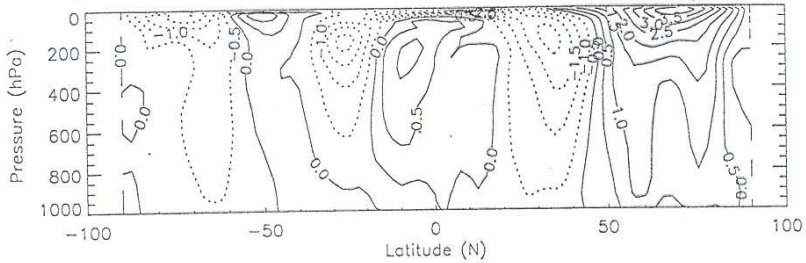

QBO

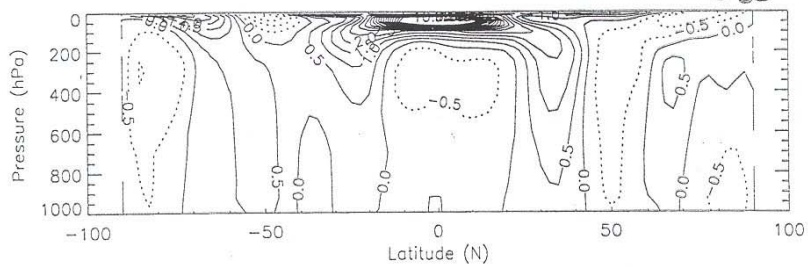

ENSO

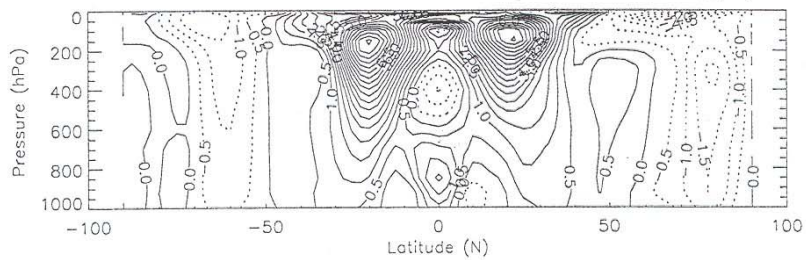

VOL

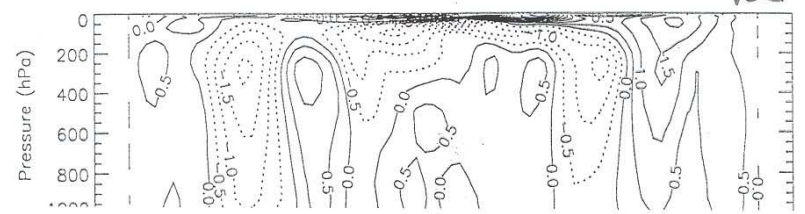

NCEP 1958-1997 average $\bar{u}$

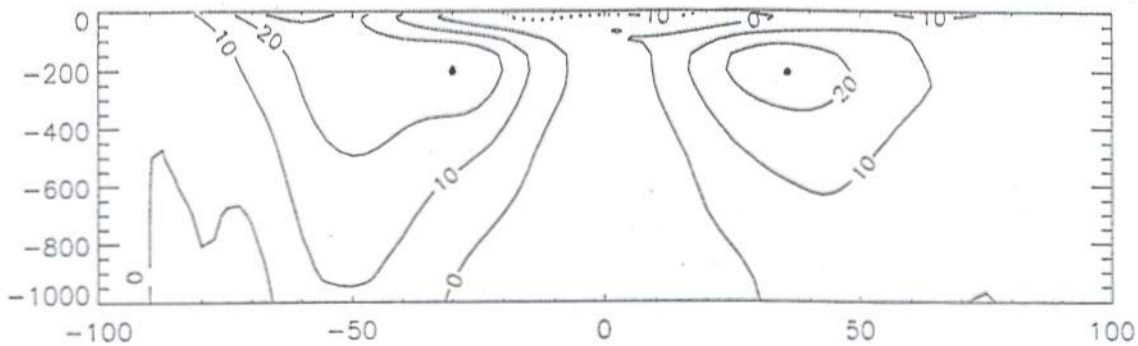

35°N ~~30°S~~ 200hPa

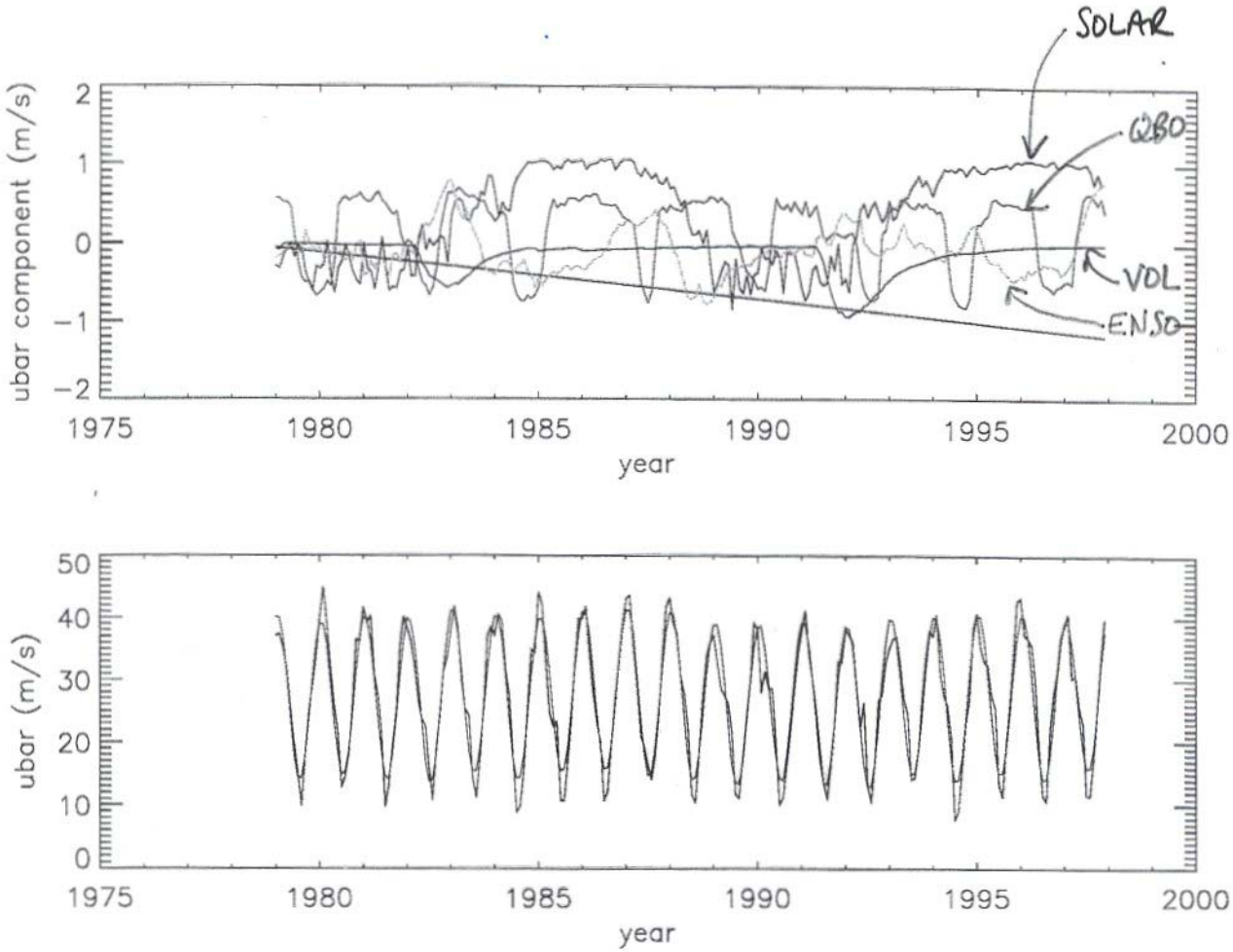

30°S, 200hPa

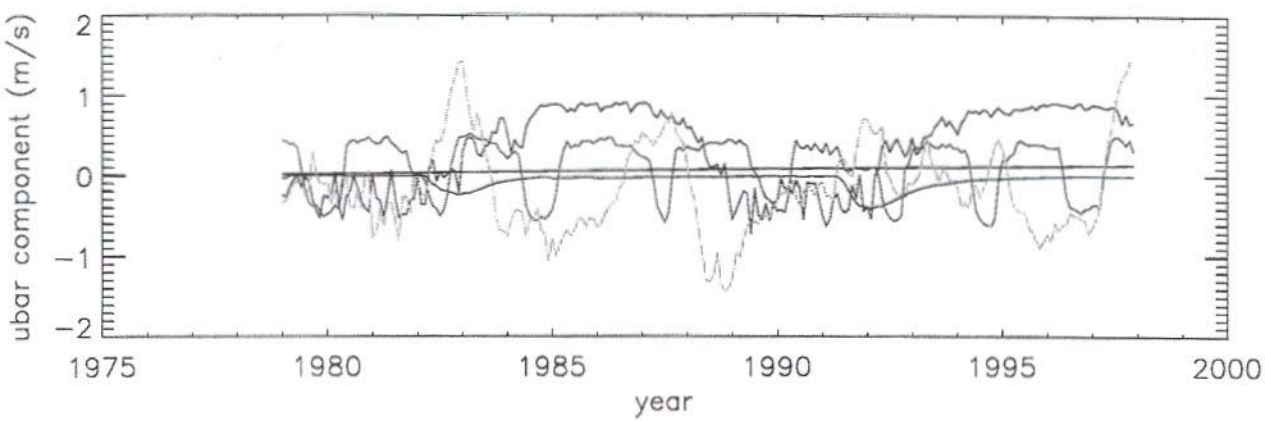
ubar component (m/s)
2
1
0
−1
−2
1975
1980
1985
1990
1995
2000
year

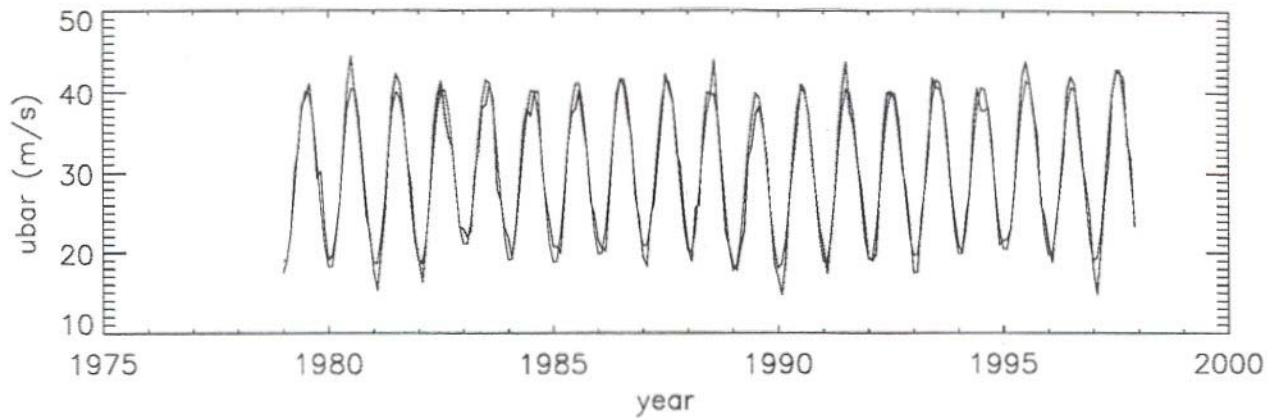
ubar (m/s)
50
40
30
20
10
1975
1980
1985
1990
1995
2000
year

MMC

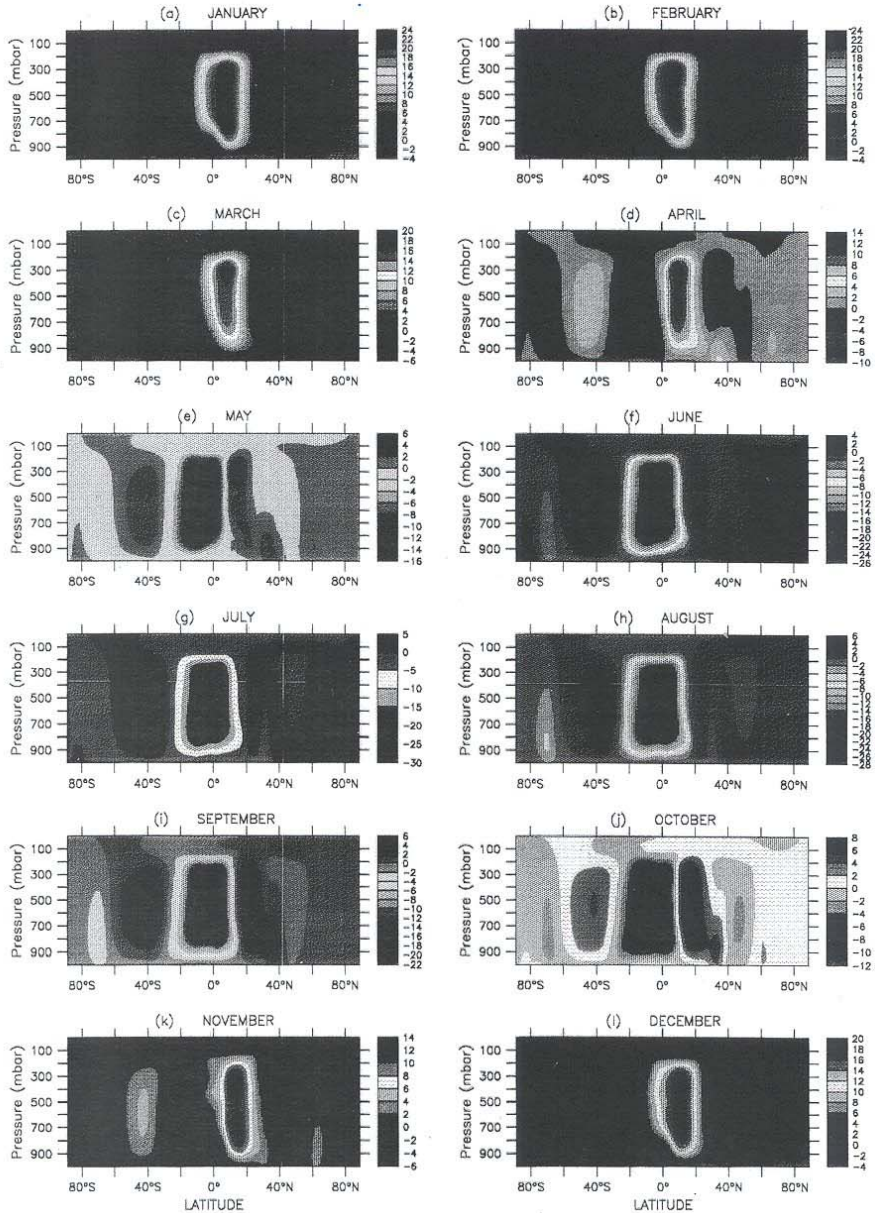
(a) JANUARY
(b) FEBRUARY
(c) MARCH
(d) APRIL
(e) MAY
(f) JUNE
(g) JULY
(h) AUGUST
(i) SEPTEMBER
(j) OCTOBER
(k) NOVEMBER
(l) DECEMBER
Pressure (mbar)
100
300
500
700
900
80°S
40°S
0°
40°N
80°N
LATITUDE

Δ MMC

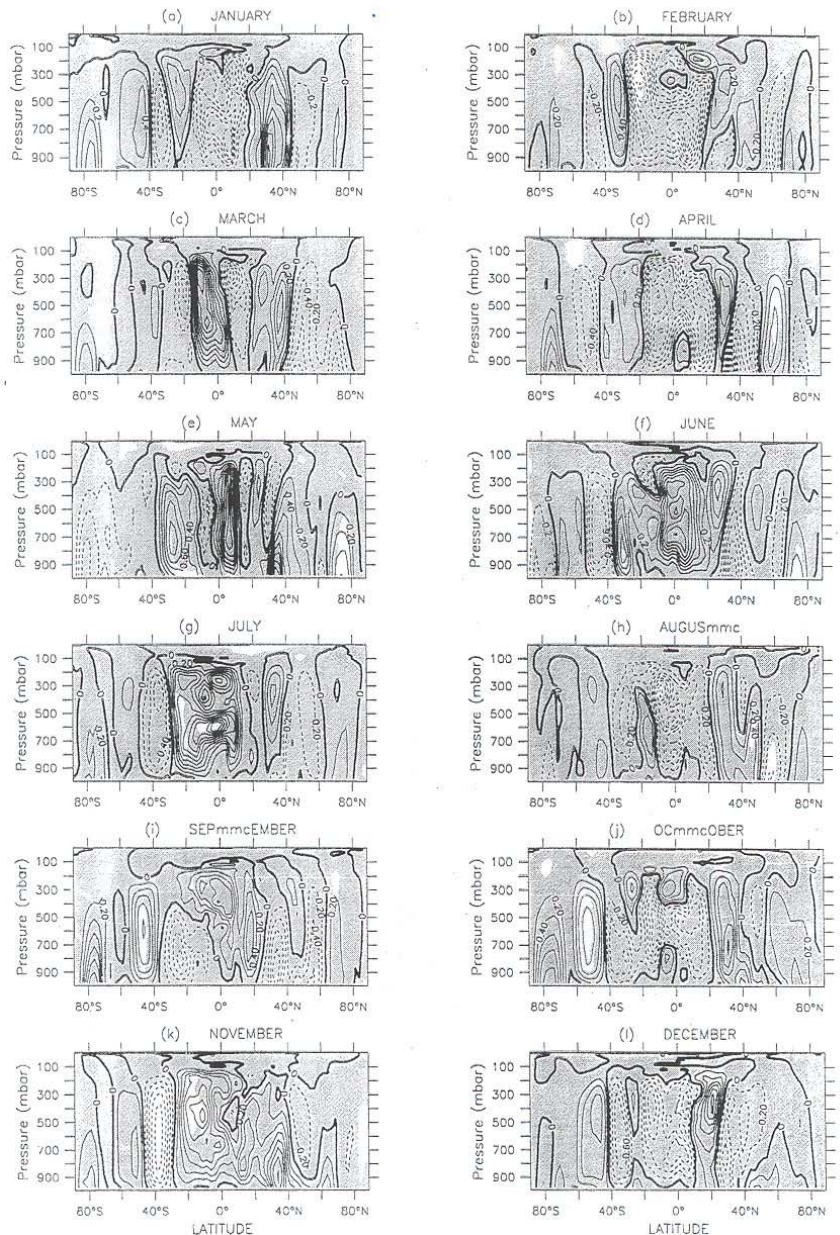
(a) JANUARY
(b) FEBRUARY
(c) MARCH
(d) APRIL
(e) MAY
(f) JUNE
(g) JULY
(h) AUGUSmmc
(i) SEPmmcEMBER
(j) OCmmcOBER
(k) NOVEMBER
(l) DECEMBER
Pressure (mbar)
100
300
500
700
900
80°S
40°S
0°
40°N
80°N
LATITUDE